Journal of Great Lakes Research 49 (2023) 229–245

Contents lists available at ScienceDirect

Journal of Great Lakes Research

journal homepage: www.elsevier.com/locate/ijglr

Spatial and temporal variations of dissolved CO_2, CH_4 and N_2O in Lakes Edward and George (East Africa)

Alberto V. Borges [a,*], William Okello [b], Steven Bouillon [c], Loris Deirmendjian [a], Angela Nankabirwa [b], Erina Nabafu [b], Thibault Lambert [a], Jean-Pierre Descy [a], Cédric Morana [a,c]

[a] Chemical Oceanography Unit, University of Liège, Liège, Belgium
[b] National Fisheries Resource Research Institute, Jinja, Uganda
[c] Department of Earth and Environmental Sciences, KU Leuven, Leuven, Belgium

ARTICLE INFO

Article history:
Received 14 May 2022
Accepted 17 November 2022
Available online 9 December 2022
Communicated by Robert Hecky

Keywords:
African Great Lakes
Lake Edward
Lake George
Carbon dioxide
Methane
Nitrous oxide

ABSTRACT

We report dissolved CO_2, CH_4 and N_2O concentrations in two large East African lakes, Edward (surface area 2,325 km^2, average depth of 37 m) and George (surface area 273 km^2, average depth of 2 m). Lake George showed modest seasonal and spatial variations, and lower partial pressure of CO_2 (pCO_2) (26 ± 16 ppm, mean ± standard deviation), CH_4 (234 ± 208 nmol/L) and N_2O saturation levels (%N_2O) (80 ± 9 %) than Lake Edward (404 ± 145 ppm, 357 ± 483 nmol/L, 139 ± 222 %). Surface waters in both lakes were over-saturated in CH_4, and Lake George was under-saturated in CO_2 while Lake Edward was slightly over-saturated in CO_2. This difference was related to higher phytoplankton biomass in Lake George than Lake Edward, with average chlorophyll-a concentrations of 177 ± 125 and 18 ± 25 μg/L, respectively. Permanent high cyanobacterial biomass in Lake George led to uniform dissolved CO_2, CH_4 and N_2O concentrations. In surface waters of Lake Edward, spatial variations of pCO_2, CH_4 and N_2O were related to bottom depth, and locally (in particular in Katwe Bay) also related to the inputs of water from Lake George via the Kazinga Channel, a 40-km natural channel connecting the lakes. Short-term mixing events related to storms increased CO_2, CH_4 and N_2O content in surface waters, in particular for CH_4 and N_2O. This indicates that mixing events in response to storms can create 'hot moments' for CH_4 and N_2O emissions to the atmosphere in tropical lakes, given the weaker vertical density gradients compared to higher latitude systems.

Introduction

Emissions of CO_2 and CH_4 from lakes and rivers to the atmosphere could be significant for global budgets (Raymond et al., 2013; Rosentreter et al., 2021). Yet, emission estimates remain uncertain for several reasons, among which, the under-representation of tropical systems in global datasets. The contribution of tropical rivers to CO_2 emissions could be disproportionately important compared to rivers at higher latitude (Raymond et al., 2013; Borges et al., 2015a; Lauerwald et al., 2015; Liu et al., 2022), as CO_2 levels and riverine surface area are higher than in temperate and boreal systems. The few data available for rivers and lakes in the tropics were up to now mainly available in South America and in particular in the Amazon river network (including floodplain lakes) (Richey et al., 1998; Richey et al., 2002; Melack et al., 2004; Abril et al., 2014; Barbosa et al., 2016; Barbosa et al., 2020; Amaral et al., 2018; Amaral et al., 2022). Several datasets in rivers have been reported recently in Africa (Borges et al., 2015a,b; Borges et al., 2019; Teodoru et al., 2015; Geeraert et al., 2017), Australia (Duvert et al., 2019), and Asia (Wit et al., 2015; Bange et al., 2019; Begum et al., 2021). These studies showed that fluvial CO_2 and CH_4 levels depend on climate that influences both the vegetation type in the catchment (savannah under semi-arid climate versus evergreen forest or peatland under humid climate), as well as the extent of riparian wetlands (flooded forest and floating macrophytes) (Abril et al., 2014; Borges et al., 2015b; Liu et al., 2022). There are less data for CO_2 in lakes, but we recently reported a relatively extensive and methodologically consistent dataset from 24 sub-Saharan African lakes (Borges et al., 2022a). We showed that the CO_2 levels in African lakes were lower than those previously assumed in the literature to be representative of tropical lakes, possibly due to an over-representation of floodplain lakes from the Amazon River network in previous studies, as well as possible methodological over-estimation of CO_2 levels computed from pH and total alkalinity (TA), due to errors on the determination of

* Corresponding author.
E-mail address: alberto.borges@uliege.be (A.V. Borges).

https://doi.org/10.1016/j.jglr.2022.11.010
0380-1330/

both pH and TA (Abril et al., 2015; Liu et al., 2020). We additionally showed that the variation of CO_2 content across different lakes was strongly controlled by the levels of primary production that itself was a function of depth and content of humic dissolved organic matter. The CO_2 content was lower in productive lakes that were shallower and with a low content of humic dissolved organic matter, in general agreement with well-established paradigms of ecological functioning of lakes, and in particular regarding the balance between gross primary production and ecosystem respiration (del Giorgio and Peters, 1994; Sand-Jensen and Staehr, 2007). We also showed that the dissolved CH_4 concentration was generally higher in African lakes than boreal ones but, in contrast, N_2O emissions from African lakes were found to be very low, due to low dissolved inorganic nitrogen content, and removal of N_2O by sedimentary denitrification.

Spatial and seasonal variations of CO_2, CH_4 and N_2O emissions from lakes have been documented in temperate and boreal systems (Huttunen et al., 2003; Karlsson et al., 2013; Denfeld et al., 2015). They follow predictable seasonal patterns related to seasonal changes in stratification and vertical mixing, lake freezing and melting for the higher latitude systems, and phytoplankton growth during the warmest and sunniest periods of the year. Emissions of CO_2 and CH_4 are generally higher in the littoral zone due a closer coupling with the sediments and the influence of macrophytes (DelSontro et al., 2018; Desrosiers et al., 2021).

The spatial and temporal variations of CO_2, CH_4 and N_2O emissions in tropical lakes have been less documented than in temperate and boreal climatic zones. Tropical systems are expected to follow different seasonal patterns due to year-round warm and high irradiance conditions, as well as physical conditions (thermal gradients and evaporation rates) less favorable for the establishment of seasonal stratification such as found in temperate and Arctic lakes (Lewis, 1987; MacIntyre, 2013). Tropical lakes often have strong diel variations in stratification and mixing in the upper water, though persistent stratification and/or seasonal mixing can develop in deeper lakes.

Spatial variations of CO_2, CH_4 and N_2O emissions have not been frequently studied in natural lakes with a few exceptions (Borges et al., 2011; Borges et al., 2014; Schilder et al., 2013; Amaral et al., 2018; Amaral et al., 2022; Barbosa et al., 2020). Spatial gradients in CO_2, CH_4 and N_2O emissions are marked in reservoirs (Beaulieu et al., 2016), although this information is not necessarily transposable to natural lakes. The CO_2 and CH_4 emissions from reservoirs are sustained in part by flooded, formerly terrestrial biomass and soils during the first years following impounding (Abril et al., 2005), and change with reservoir age (Barros et al., 2011). Additionally, natural lakes and reservoirs differ in morphometry (Sjöberg et al., 2022); in particular, the higher drainage area to surface area ratio of reservoirs leads to higher sediment transport and loading to reservoirs than in lakes (Abraham et al., 1999). This might contribute to differences in aquatic carbon cycling, such as sedimentation rates of organic matter (Mendonça et al., 2017) and, consequently, also CO_2 and CH_4 emissions.

Here, we report data on dissolved CO_2, CH_4 and N_2O concentrations in Lakes Edward and George, two large East African lakes (Fig. 1). We studied vertical and horizontal gradients, obtained during 4 cruises, as well as a 3-year regular monitoring (every 21 d) at a shallow and a deeper station in Lake Edward.

Material and methods

Site description

Lake Edward is located along the border between Uganda and the Democratic Republic of the Congo (DRC) in the western arm of the East African rift valley. It is located 912 m above sea level, has a maximum depth of 117 m, a mean depth of 37 m, and a surface area of 2,325 km^2 (Russell and Johnson, 2006). The catchment has a total surface area of 20,370 km^2 and is covered in the lowlands by a mosaic of East African evergreen bushland, secondary *Acacia* wooded grassland, and farmland, and in the highlands by afromontane forest, ericaceous scrub and high montane moorland (with increasing altitude) (Beuning and Russell, 2004). Principal inflows to Lake Edward derive from the Rwenzori Mountains to the north (Nyamugasani and Lubilja Rivers), the Kigezi highlands to the east, and the Virunga volcanoes to the south (Rutshuru, Ishasha, and Rwindi Rivers). The lake drains to Lake Albert via the Semliki River, through the Ituri forest, and loses by evaporation ~50 % of its total water input (Russell and Johnson, 2006). Mean annual precipitation in the Edward basin is approximately 900 mm y^{-1} falling in two rainy seasons coinciding with the passing of the intertropical convergence zone, from October to December and March to May. (Russell and Johnson, 2006). Lake Edward is connected to Lake George to the east by the Kazinga Channel, a 40 km long drowned river valley. Lake George is smaller (273 km^2) and shallower, with a maximum depth of only 3 m (Ganf and Viner, 1973; Viner and Smith, 1973).

Field cruises and regular monitoring

We sampled Lake Edward, Kazinga Channel and Lake George on four occasions (20/10–07/11/2016, 23/03–08/04/2017, 18/01–02/02/2018, 21/03–30/03/2019). During each cruise, sampling was designed to cover spatial variability horizontally and was mainly confined to Ugandan territorial waters (Fig. 1), allowing sampling to 30 m, with the exception of the sampling cruise in January 2018 when the deepest part of the lake was sampled in the territorial waters of the DRC (Fig. 1). From January 2017 to December 2019, a shallow station (3 m bottom depth) and a deeper station (22 m bottom depth) were regularly sampled, every 21 d in 2017 and 2018, and every 30 d in 2019. Water collection was carried out with the boat of the Katwe Marine Police, during day-time; from mid-morning to mid-afternoon during the cruises, and in the majority of cases during the morning (09:00 to 11:00 local time) during the regular monitoring (shallow and deeper station).

Solar radiation, ultraviolet radiation, wind speed (cup anemometer), wind direction (wind vane), rain (tipping bucket rain gauge), air temperature, barometric pressure data were acquired with a Davis Instruments weather station (Vantage Pro2 fitted with standard sensors from the manufacturer) in Mweya on top of a building of the Uganda Wildlife Authority, 4 m above ground (−0.190384°N 29.899103°E). Data were measured every 5 s, averaged and logged every 10 min with a Davis Instruments Envoy 8X logger and downloaded on a personal computer at the end of each sampling cruise.

Continuous measurements

During the March 2019 cruise, continuous measurements (1 min interval) of partial pressure of CO_2 (pCO_2) and of partial pressure of CH_4 (pCH_4) were made with an equilibrator designed for turbid waters consisting of a tube filled with glass marbles (Frankignoulle et al., 2001) coupled to a Los Gatos Research off-axis integrated cavity output spectroscopy analyzer (Ultraportable Greenhouse Gas Analyzer with extended range for CH_4). In parallel, water temperature, specific conductivity, pH, dissolved oxygen saturation level ($\%O_2$), turbidity, chlorophyll-*a* (Chl-*a*), and fluorescent dissolved organic matter (FDOM) were measured with an YSI eXO-II multi-parameter probe, positioned with a Garmin geographical position system (Map 60S) portable probe, and depth with a Humminbird Helix 5 echo-sounder. The Chl-*a* signal of the eXO-II was calibrated by linear regression against discrete measurements of

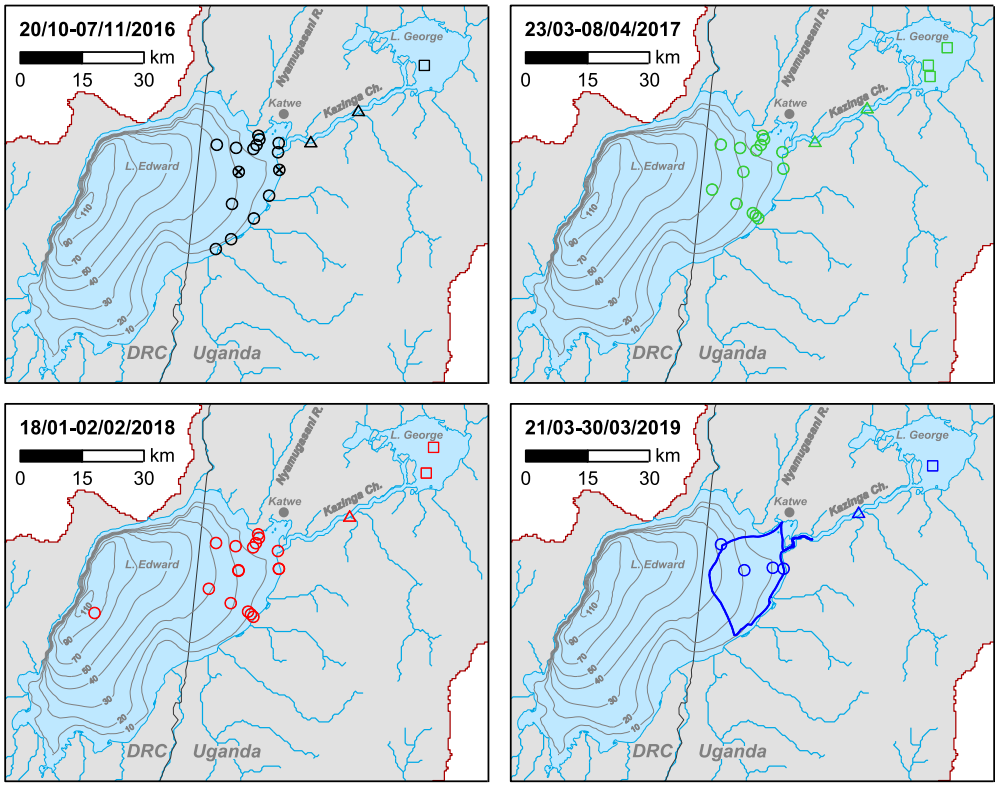

Fig. 1. Map of Lake Edward and George showing catchment (grey), and large rivers (Strahler order ≥ 2), border between Uganda and Democratic Republic of Congo (RDC, black line), bathymetry and sampling stations (circles) in October 2016, March 2017, January 2018, March 2019, as well as continuous measurements in surface waters in March 2019. Crosses in the map of October 2016 indicate the two stations that were chosen for the regular monitoring (2017–2019).

Chl-*a* measured by high performance liquid chromatography (HPLC) (see below). The data were not corrected for fluorescence quenching (Marra 1997), given the wide range of variations of Chl-*a*, and that measurements were made during day-time (early-morning to mid-afternoon) (no day-night variations) and in surface waters only (no vertical profiles). Surface water was pumped to the equilibrator and the multi-parameter probe (on deck) with a 12 V-powered water pump (LVM105) attached to the side of the boat at a fixed depth of about 0.5 m depth.

The response time of eXO-II sensors was considered immediate given the time interval of data logging (1 min). The design of equilibrator we used for the continuous CO_2 and CH_4 measurements has an equilibration time constant ≤1 min for CO_2 (Frankignoulle et al., 2001; Santos et al., 2012; Webb, 2016) and 15 min for CH_4 (Webb, 2016). The pCO_2 and eXO-II data were considered as immediate, while the time of the CH_4 data was adjusted by 15 min, as commonly applied for continuous measurements of CH_4 with an equilibrator (Tait et al., 2017; Call et al., 2018; Wells et al., 2020; Reading et al., 2021; Ollivier et al., 2022).

During the March 2019 cruise, we deployed a mooring at a station at 10 m bottom depth in Lake Edward (−0.2459°N 29.8635°E) equipped with RBR Solo temperature sensors at 6 depths from surface to 1 m above the sediment (0.2, 1.0, 2.0, 5.0, 7.5 and 9.0 m depth). Temperature data were logged every 10 min from 21/03/2019 (13:00 local time (LT)) to 23/03/2019 (13:50 LT), with a resolution of 0.00005 °C and an accuracy of ± 0.002 °C (manufacturer's specifications).

Discrete sampling

Sampling was done from the side of the boat with a 5.0 L Niskin bottle (General Oceanics). During the first cruise, vertical profiles of water temperature, specific conductivity, pH, $\%O_2$ and Chl-*a* were measured with a Hydrolab DS5 multi-parameter probe, while during the other three cruises and also during the monitoring, turbidity and FDOM were measured additionally with a YSI eXO-II multi-parameter probe. The resolution and accuracy of the temperature measurements were according to the specifications from the manufacturers, respectively: 0.01 °C and ±0.10 °C for the Hydrolab DS5 probe; 0.001 °C and ±0.01 °C for the YSI eXO-II probe. The data were logged with the smallest possible time interval of 1 and 5 s for the YSI eXO-II and the Hydrolab DS5 probes, respectively. The vertical resolution of the profiles was typically ~0.02 and ~0.1 m for the YSI eXO-II and the Hydrolab DS5 probes, respectively. Both multi-parameter probes were calibrated according to manufacturer's specifications, in air for $\%O_2$ and with standard solutions for other variables: commercial pH buffers (4.00, 7.00, 10.00), a 1000 µS cm^{-1} standard for conductivity. pCO_2 was measured directly after water sampling with a Li-Cor Li-840 infra-red gas analyser (IRGA) based on the headspace technique with 4 polypropylene 60 ml syringes (Abril et al., 2015). The Li-Cor 840 IRGA was calibrated before and after each cruise with ultrapure N_2 and a suite of gas standards (Air Liquide Belgium) with CO_2 mixing ratios of 388, 813, 3788 and 8300 ppm. The overall precision of pCO_2 measurements was ±2.0 %.

Sample conditioning and laboratory analysis

Samples for CH_4 and N_2O were collected from the Niskin bottle with a silicone tube in 60 ml borosilicate serum bottles (Wheaton), poisoned with 200 µL of a saturated solution of $HgCl_2$ and sealed with a butyl stopper and crimped with an aluminium cap. Measurements were made with the headspace technique (Weiss, 1981) and a gas chromatograph (GC) (SRI 8610C) with a flame ionisation detector for CH_4 and electron capture detector for N_2O calibrated with CO_2:CH_4:N_2O:N_2 gas mixtures (Air Liquide Belgium) with mixing ratios

of 1, 10 and 30 ppm for CH_4, 404, 1018, 3961 ppm for CO_2, and 0.2, 2.0 and 6.0 ppm for N_2O. The precision of measurement based on duplicate samples was ±3.9 % for CH_4 and ±3.2 % for N_2O. The CO_2 concentration is expressed as partial pressure in parts per million (ppm) and CH_4 as dissolved concentration (nmol/L), in accordance with convention in existing topical literature. Variations of N_2O were modest and concentrations fluctuated around atmospheric equilibrium, so data are presented as percent of saturation level (%N_2O), where atmospheric equilibrium corresponds to 100 %, computed from the global mean N_2O air mixing ratios given by the Global Monitoring Division (GMD) of the Earth System Research Laboratory (ESRL) of the National Oceanic and Atmospheric Administration (NOAA) (https://www.esrl.noaa.gov/gmd/hats/combined/N2O.html), and using the Henry's constant given by Weiss and Price (1980).

Samples for the stable isotope composition of CH_4 (δ^{13}C-CH_4) were collected and preserved as described above for the CH_4 concentration. The δ^{13}C-CH_4 was determined with a custom developed interface, whereby a 20 ml He headspace was first created, and CH_4 was flushed out through a double-hole needle, non-CH_4 volatile organic compounds were trapped in liquid N_2, CO_2 was removed with a soda lime trap, H_2O was removed with a magnesium perchlorate trap, and the CH_4 was quantitatively oxidized to CO_2 in an online combustion column similar to that of an elemental analyzer. The resulting CO_2 was subsequently pre-concentrated by immersion of a stainless steel loop in liquid N_2, passed through a micropacked GC column (Restek HayeSep Q, 2 m length, 0.75 mm internal diameter), and finally measured on a Thermo DeltaV Advantage isotope ratio mass spectrometer (IRMS). Calibration was performed with CO_2 generated from certified reference standards (IAEA-CO-1 or NBS-19, and LSVEC) and injected in the line after the CO_2 trap. Reproducibility of measurement based on duplicate injections of samples was typically better than ±0.5 ‰.

Water was filtered on Whatman glass fibre filters (GF/F grade, 0.7 μm porosity) for particulate organic carbon (POC) and Chl-*a* (47 mm diameter). Filters for POC were stored dry and filters for Chl-*a* were stored frozen at −20 °C. Filters for POC analysis were decarbonated with HCl fumes for 4 h and dried before encapsulation into silver cups; POC concentration was analysed on an EA-IRMS (Thermo FlashHT with DeltaV Advantage), with a reproducibility better than ±5 %. Data were calibrated with certified (IAEA-600: caffeine) and in-house standards (leucine and muscle tissue of Pacific tuna) that were previously calibrated versus certified standards. The Chl-*a* samples were analysed by HPLC according to Descy et al. (2005), with a reproducibility of ±0.5 % and a detection limit of 0.01 μg/L. Part of the Chl-*a* data were previously reported by Stoyneva-Gaertner et al. (2020).

The water filtered through GF/F Whatman glass fibre filters was collected and further filtered through polyethersulfone syringe encapsulated filters (0.2 μm porosity) for nitrate (NO_3^-), nitrite (NO_2^-) and ammonium (NH_4^+) and were stored frozen (−20 °C) in 50 ml polypropylene vials. NO_3^- and NO_2^- were determined with the sulfanilamide colorimetric with the vanadium reduction method (APHA, 1998), and NH_4^+ with the dichloroisocyanurate-salicylate-nitroprussiate colorimetric method (Standing committee of Analysts, 1981). Detection limits were 0.3, 0.01, and 0.15 μmol/L for NH_4^+, NO_2^- and NO_3^-, respectively. Precisions were ±0.02 μmol/L, ±0.02 μmol/L, and ± 0.1 μmol/L for NH_4^+, NO_2^- and NO_3^-, respectively.

The time-sampled and geo-referenced data-sets reported in this work are publically available (Borges et al. 2022b).

Results and discussion

From June 2016 to March 2019, the weekly mean of air temperature ranged between 22.0 and 26.6 °C and averaged 24.1 ± 1.0 °C (mean ± standard deviation) and the weekly mean of wind ranged between 0.9 and 2.0 m s^{-1} and average 1.3 ± 0.2 m s^{-1} (Eletronic Supplementary Material (ESM) Fig. S1). The first two sampling cruises (October 2016 and March 2017) corresponded to the start and the end of the rainy season, respectively. The last two sampling cruises (January 2018 and March 2019) both corresponded to the end of the dry season. The two first cruises were characterized by lower air temperature and wind, but higher humidity and precipitation than the two last cruises (ESM Fig. S1).

Vertical variations

We sampled the western and deepest part of Lake Edward in February 2018 (Fig. 1). A superficial thermocline was observed between 0 and 20 m, as well as a second thermocline between 61 and 65 m (Fig. 2). This second thermocline coincided with the base of the chemocline, as shown by the gradient of specific conductivity, and of the oxycline both situated between 56 and 63 m (Fig. 2). Yet, the vertical temperature gradient in February 2018 was weak compared to previous profiles obtained in this part of the lake (Beadle, 1932; 1966; Damas 1937; ESM Fig. S2). Whole water-column average temperature (25.7 ± 0.1 °C) in the deepest part of the lake (Fig. 2) was close to bottom water temperature (25.8 °C) observed, also in February 2018, on the eastern part of the lake at 30 m bottom depth (corresponding to fully mixed conditions) (Fig. 3). Vertical gradients of conductivity from surface to 70 m depth were weaker in February 2018 than along a previously reported vertical profile (ESM Fig. S2). Taken together, these observations suggest that, in February 2018 (Fig. 2), we sampled the lake after a recent overturn and vertical homogenization. While previously reported vertical profiles show thermal stratification and anoxic bottom waters (ESM Fig. S2), lake overturn and full oxygenation to the bottom of the lake was mentioned by Verbeke (1957) during the particularly cold and stormy dry season of 1953.

In February 2018, surface waters of Lake Edward were close to oxygen saturation, and waters were anoxic below 63 m (Fig. 2). The pCO_2 values in surface waters (~430 ppm) were marginally above atmospheric equilibrium (~390 ppm), gradually increased to ~540 ppm at 50 m (below the seasonal thermocline), and then steadily increased across the oxycline and into deeper anoxic water for a maximum of 1,150 ppm at 85 m. CH_4 was above atmospheric equilibrium (~2 nmol/L) throughout the water column, with slightly higher values (58 nmol/L) within the top 20 m than between 20 m and 50 m (19–33 nmol/L), and then steadily increased by several orders of magnitude for a maximum of 86,934 nmol/L at 85 m. NO_2^- and NO_3^- were undetectable in anoxic waters (putatively due to denitrification) and increased across the oxycline, with NO_2^- peaking at the top of the oxycline (0.8 μmol/L at 55 m) and NO_3^- peaking (2.7 μmol/L) at 40 m, putatively due to nitrification as indicated by the consistent decrease in NH_4^+ from 39.9 μmol/L at 85 m to 0.8 μmol/L at 40 m. Above their respective peaks, NO_3^- and NO_2^- steadily decreased towards surface waters. Surface waters were close to saturation in N_2O (%N_2O ~99 %), and slightly under-saturated in the anoxic waters (%N_2O between 96 and 98 %). Two peaks of N_2O leading to over-saturations seem to be related to nitrification as the first peak at 55 m coincided with the NO_2^- peak (%N_2O ~105 %) and the second larger peak at 40 m (%N_2O ~115 %) coincided with the NO_3^- maximum.

Fig. 3 shows the vertical profiles at 32 m bottom depth in Lake Edward obtained during the four cruises (Fig. 1). Conditions were stratified in October 2016 and March 2017 corresponding to the rainy season (ESM Fig. S1) with a thermocline situated at between ~16 and ~22 m, and anoxic conditions in bottom waters (Fig. 3). The weaker or nearly absent vertical gradients of dissolved O_2 and water temperature indicated partly mixed and fully mixed conditions in March 2019 and January 2018 (Fig. 3 and ESM

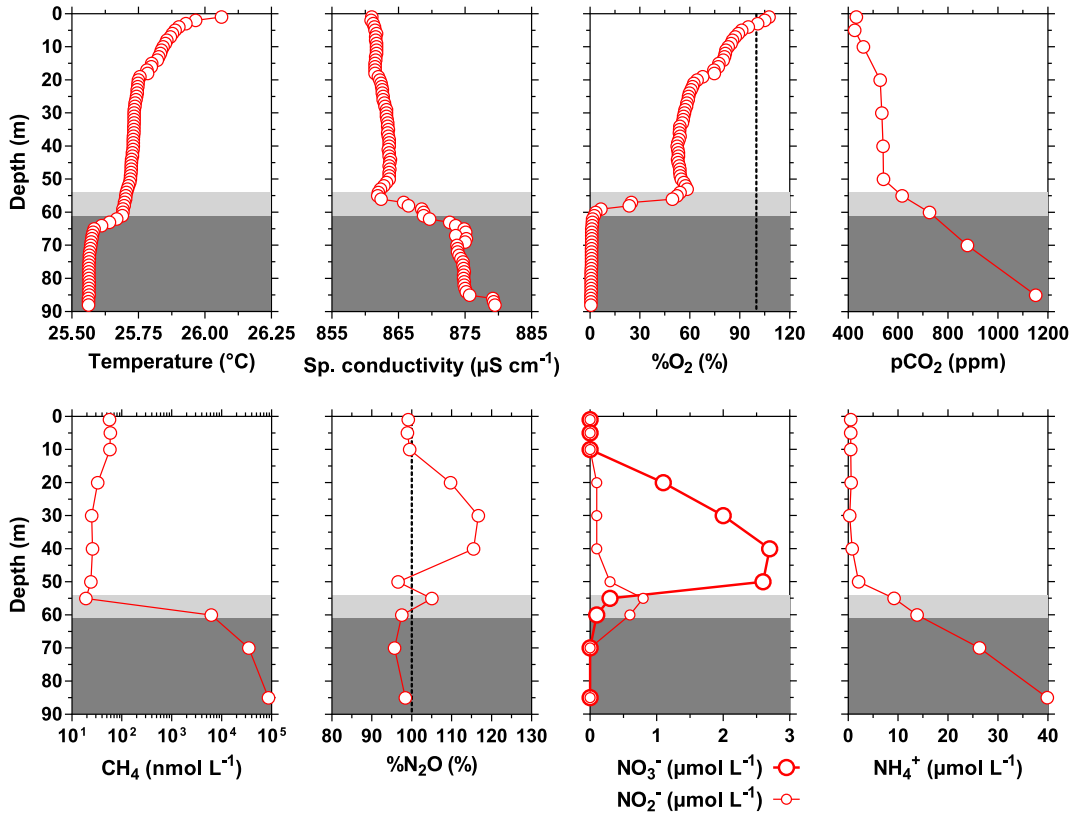

Fig. 2. Vertical profiles of water temperature (°C), specific (Sp.) conductivity (µS cm^{-1}), O_2 saturation level (%O_2, %), partial pressure of CO_2 (pCO_2, ppm), CH_4 concentration (nmol/L), N_2O saturation level (%N_2O, %), NO_3^-, NO_2^- and NH_4^+ concentrations (µmol/L) in Lake Edward (90 m bottom depth) on 02/02/2018 at 12:30 (local time). Light and darker grey indicate the oxycline, and anoxic layer, respectively. Vertical dotted line indicates the atmospheric equilibrium value.

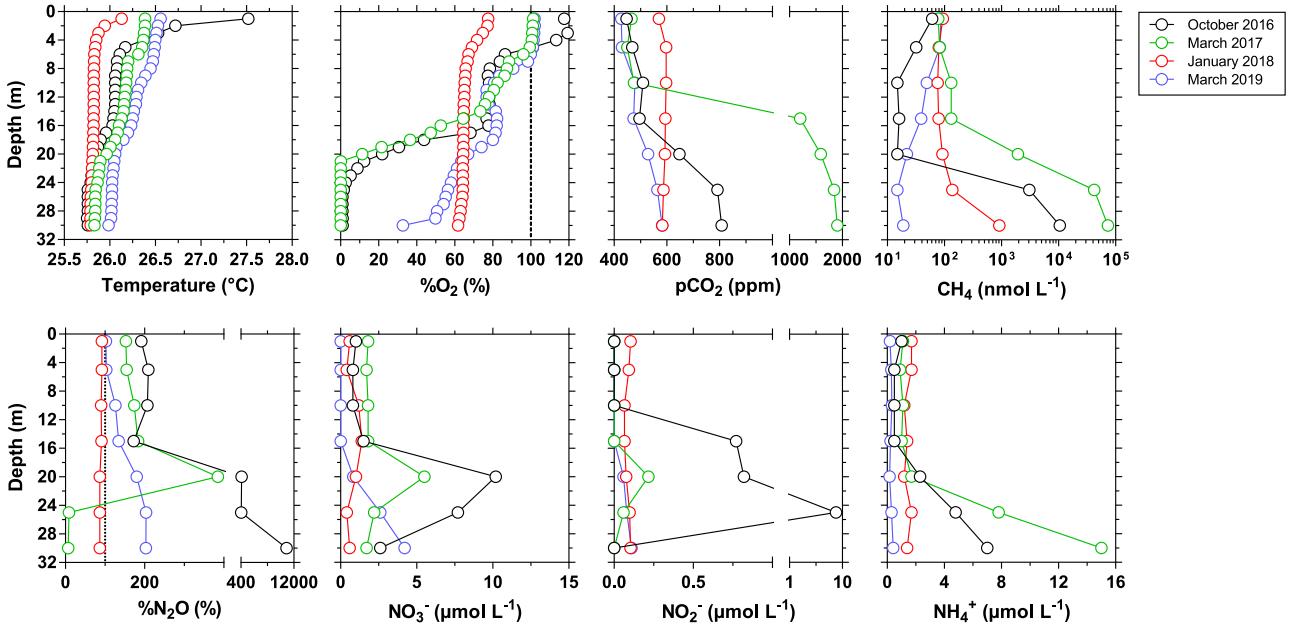

Fig. 3. Vertical profiles of water temperature (°C), O_2 saturation level (%O_2, %), partial pressure of CO_2 (pCO_2, ppm), CH_4 concentration (nmol/L), N_2O saturation level (%N_2O, %), NO_3^-, NO_2^- and NH_4^+ concentrations (µmol/L) in Lake Edward (32 m bottom depth) in October 2016 (25/10/2016 at 13:10 local time (LT)), March 2017 (25/03/2017 at 09:20 LT), January 2018 (19/01/2018 at 11:55 LT), March 2019 (30/03/2019 at 10:00 LT). Vertical dotted line indicates the atmospheric equilibrium value.

Fig. S2), respectively, corresponding to the two cruises carried out at the end of the dry season (ESM Fig. S1). During the stratified conditions, specific conductivity (ESMFig. S3), pCO_2, CH_4 and NH_4^+ (Fig. 3) increased with depth, with the highest values in bottom waters in March 2017. CH_4 and NH_4^+ were nearly homogeneous with depth during the two dry season conditions – January 2018 and March 2019 (Fig. 3). Observations of pCO_2, %N_2O and NO_3^- increased slightly with depth in March 2019 (partly mixed condi-

tions) indicating some organic matter degradation and nitrification in bottom waters. The $\%N_2O$ in bottom waters was different during the two rainy seasons, with a marked over-saturation in October 2016 (10,389 %, start of the rainy season) and a strong under-saturation in March 2017 (7 %, end of the rainy season). We hypothesize that this pattern resulted from the timing of the sampling with regards to the onset (and duration) of the anoxia in bottom waters. During the early rainy season (October 2016), anoxic conditions were presumably only recently established, while anoxic conditions were well established during the late rainy season (March 2017). This could explain intense N_2O production in bottom water from nitrification that also resulted in a very large peak in NO_2^- and higher NO_3^- in bottom water in October 2016 compared to March 2017. Incomplete denitrification at low O_2 levels (Codispoti and Christensen, 1985; Mengis et al., 1997) might also have contributed to the production and accumulation of N_2O in bottom waters with the onset of anoxia in October 2016. Under well-established anoxic conditions in bottom waters (March 2017), N_2O was removed from the water column by putative sedimentary or pelagic denitrification, leading to under-saturation in N_2O. In March 2017, under partly mixed conditions, N_2O peaked at the oxycline along with NO_2^- and NO_3^-, while $\%N_2O$, NH_4^+, NO_3^- and NO_2^- were relatively homogeneous throughout the water column, under fully mixed conditions in January 2018. In the deeper part of the lake, N_2O was close to saturation in the anoxic bottom waters in February 2018 (Fig. 2). This might result from the fact that anoxia had only been recently established (after a lake overturn), so that N_2O had not yet been significantly removed by denitrification, as it occurred in March 2017 at 30 m bottom depth (under well-established anoxic conditions).

At the station of 30 m bottom depth, variations from cruise to cruise were much more modest in surface water than at depth (Fig. 3). The surface water dissolved CH_4 concentrations varied little between the four cruises (61–94 nmol/L); pCO_2 was higher during fully mixed conditions (January 2018, 570 ppm) compared to the other three cruises (427–466 ppm), while $\%N_2O$ was higher during the two stratified conditions (with anoxic bottom waters, 192–152 %) compared to the other cruises with more mixed conditions (with oxic bottom waters, 92–102 %).

Horizontal variations

In Lake Edward, surface water with a lower specific conductivity (202–726 μS cm^{-1}) was observed at the mouth of the Kazinga Channel than in the rest of the lake, and this water mass propagated northward towards Katwe Bay and also to lesser extent southward of the mouth of the Kazinga Channel during the two cruises at the end of the dry season (Fig. 4). Elsewhere in Lake Edward, specific conductivity in surface waters was higher than in Katwe Bay and relatively homogenous (853 ± 10 μS cm^{-1}). Surface water from the Kazinga Channel had characteristics close to those in Lake George, with high Chl-*a* (177 ± 125 μg/L), low pCO_2 (28 ± 13 ppm), CH_4 (135 ± 102 nmol/L) and $\%N_2O$ (77 ± 10 %) (Fig. 5). The high phytoplankton biomass in Lake George, dominated by cyanobacteria, was related to its shallowness (<3 m) compared to Lake Edward (Stoyneva-Gaertner et al., 2020) and led to a strong uptake of CO_2 and consequently low pCO_2 values down to 13 ppm, among the lowest values reported in the literature for lakes (e.g. Sobek et al., 2005). The high phytoplankton biomass should also provide substantial quantities of organic matter to the sediment which should lead to intense denitrification and removal of N_2O from the water column, leading to N_2O under-saturation in surface waters. Indeed, the organic carbon content in surface (0–5 cm) sediments of Lake George was 34.5 %, distinctly higher than in the littoral zone (5 m bottom depth) of Lake Edward (13.3 %) (not shown, Bouillon and Morana, unpublished). In Lake George, the sediments are, according to Viner and Smith (1973), sharply stratified, with a layer of soft, richly organic mud up to about 2.5 m thick, overlying the deposits of an earlier lake. The high phytoplankton biomass also led to CH_4 fluxes from the sediment to the water column (by both diffusion and dissolution of rising bubbles) that were one order of magnitude higher in Lake George than in Lake Edward (Morana et al., 2020). Surprisingly, the CH_4 concentrations in surface waters of Lake George and Kazinga Channel were of the same order of magnitude than in Lake Edward (Fig. 5). This contradiction was related to much higher CH_4 microbial oxidation measured with incubations (data not shown) in Lake George than in Lake Edward, that seemed related to the activity of methanotrophs fixed on aggregates and cyanobacteria colonies (Borges et al., unpublished data). The pCO_2, CH_4 and $\%N_2O$ in surface waters of Lake George were relatively homogeneous from one cruise to another, remaining within narrow ranges (19–46 ppm, 43–336 nmol/L, 63–93 %, respectively). On March 2017, multiple samplings (n = 3) were made in Lake George and the values pCO_2, CH_4 and $\%N_2O$ were also similar (30–41 ppm, 77–124 nmol/L, 79–92 %, respectively). The uniformity of the CO_2, CH_4 and N_2O levels in space and time may result from phytoplankton exhibiting little seasonality in Lake George (Ganf and Viner, 1973; Greenwood, 1976).

The mixing of the water delivered by the Kazinga Channel with water in Lake Edward led to distinct patterns as a function of specific conductivity (Fig. 5), with a decreasing pattern for Chl-*a* and increasing pattern of pCO_2, $\%N_2O$ and CH_4. These mixing patterns were also observed in the continuous measurements of Chl-*a*, CH_4 and pCO_2 obtained during a one-day survey in March 2019 (Fig. 6).

In Lake Edward "proper" (samples with a specific conductivity > 800 μS cm^{-1}), Chl-*a*, pCO_2, CH_4 and $\%N_2O$ varied as a function of depth (Figs. 7, 8). Higher Chl-*a* values in surface waters were observed at shallower bottom depths resulting from higher primary production (Morana et al., 2022) sustained by nutrient inputs from sediments, as well as a favorable ratio of photic depth and mixed layer depth (Del Giorgio and Peeters, 1994). Higher primary production at shallower bottom depths led to low surface water pCO_2 and concomitant organic matter delivery to sediment, which probably sustained high benthic remineralization rates. This in turn led to low $\%N_2O$ values due to sedimentary denitrification and high CH_4 values due to sedimentary methanogenesis. Relationships between surface water $\%N_2O$ and CH_4 and water column depth were to some extent obscured in some cases by higher values at a bottom depth of 22 m that will discussed below, but the patterns were clear when the data was binned (Fig. 8).

These patterns of higher Chl-*a* and CH_4 and lower pCO_2 in the littoral area compared to the deeper part of Lake Edward were also observed in the continuous measurements obtained during a one-day survey in March 2019 (Fig. 6). A strong increase of CH_4 in the vicinity of the delta of the Nyamugasani River coincided with a decrease in water temperature, specific conductivity (Fig. 4), $\%O_2$ and an increase of turbidity, FDOM and pCO_2 (Fig. 9). These patterns indicate the inputs from river water consistent with the proximity of the delta of the Nyamugasani River, as well with the fact that the survey was carried out after a few days of strong storms due to the start of the rainy season. The likely increase of freshwater discharge resulting from stormy weather led to riverine inputs to Katwe Bay that should have had a high CH_4 content given the very extensive papyrus wetlands in the Nyamugasani delta.

Short-term variations

In March 2017, an extremely high value of CH_4 concentration (3,277 nmol/L) was observed in surface waters of Lake Edward at

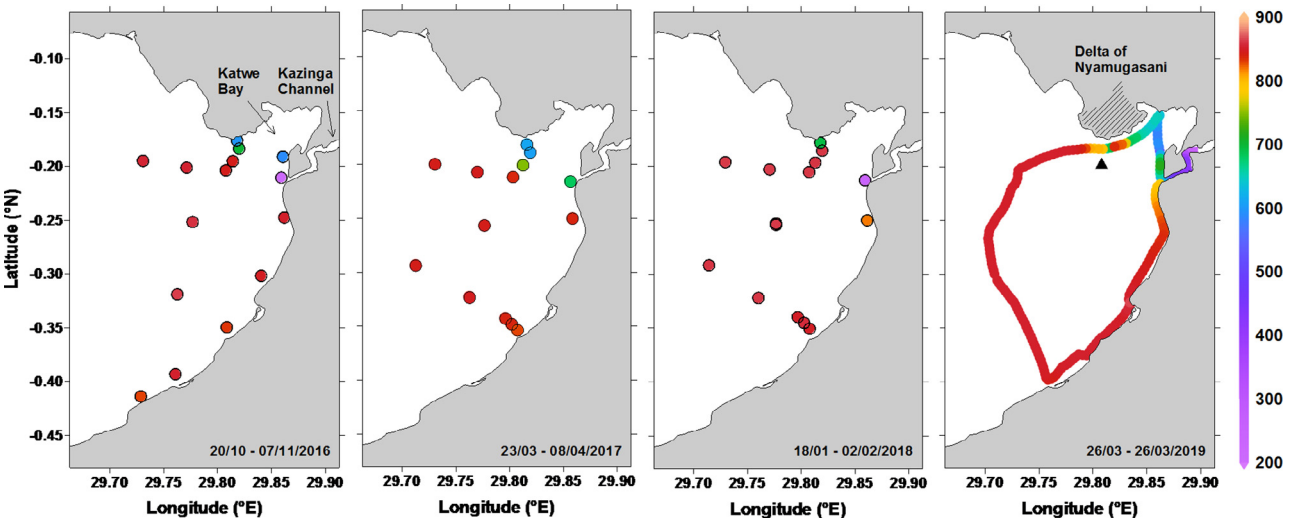

Fig. 4. Variations in surface waters of Lake Edward of specific conductivity (μS cm^{-1}) in October 2016, March 2017, January 2018, March 2019. Black triangle indicates an area presumably influenced by inputs from the Nyamugasani river.

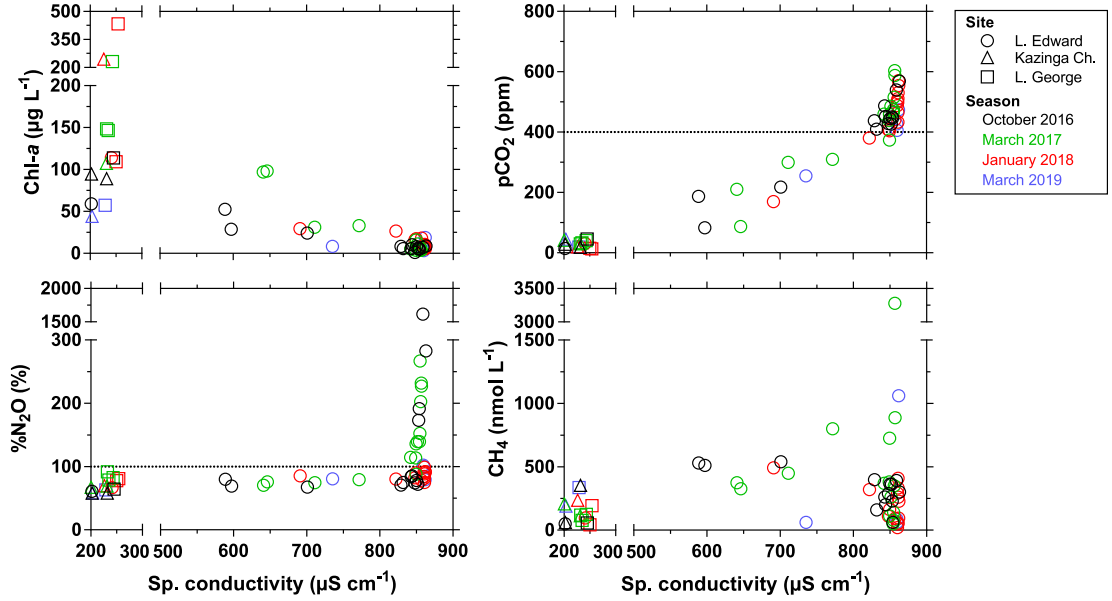

Fig. 5. Variations in surface waters of Lake Edward, Kazinga Channel and Lake George of Chlorophyll-*a* (Chl-*a*, μg/L), partial pressure of CO_2 (pCO_2, ppm), N_2O saturation level ($\%N_2O$, %), and CH_4 concentration (nmol/L) as function of specific (Sp.) conductivity (μS cm^{-1}) in October 2016, March 2017, January 2018, March 2019. Horizontal dotted line indicates the atmospheric equilibrium value.

22 m bottom depth (Fig. 7). Compared to other samples in surface waters collected during this cruise, the high CH_4 concentration was related to lower water temperature and $\%O_2$ and higher pCO_2 (Fig. 10). Additionally, CH_4 had a lighter carbon isotopic composition compared to all other samples collected in the surface waters of Lake Edward, with a δ^{13}C-CH_4 value close to the most negative one reported in bottom waters (ESM Fig. S6). This indicated that the high CH_4 concentration was related to a mixing event. Indeed, the sampling was carried out in the morning of March 30, a few hours after a night-time storm as indicated by high wind speeds (maximum 10 min average of 6.5 m s^{-1}), coinciding to a sudden decrease of air temperature of ~1.9 °C in about 20 min (ESM Fig. S4). This was confirmed by the comparison of vertical profiles obtained 3–4 days prior to the storm (March 26 and 27) that show stratified conditions at stations at 22 and 32 m bottom depth, as indicated by vertical gradients of water temperature (Fig. 11) and specific conductivity (ESM Fig. S5). On March 31, water temperature and specific conductivity were vertically uniform, although a slight gradient of both variables still persisted between 18 and 20 m depth on March 30. This homogenization of both water temperature and specific conductivity, as well as their lowering in surface waters was consistent with vertical mixing after the storm event. The higher CH_4, pCO_2, $\%N_2O$, and lower δ^{13}C-CH_4 value in the mixed layer on March 30 and 31 compared to March 26 and 27 were consistent with this mixing event in response to the storm. However, on March 30, at 20 m depth, water temperature, $\%O_2$ and $\%N_2O$ were lower and pCO_2 and CH_4 were higher than on March 26 (both stations at 22 m bottom depth). Vertical mixing alone should have led to a general decrease (or increase) of these variables in the bottom waters but not to values below (or above) those observed prior to the storm. This indicates that in addition to vertical mixing alone, there should also have been a transfer of

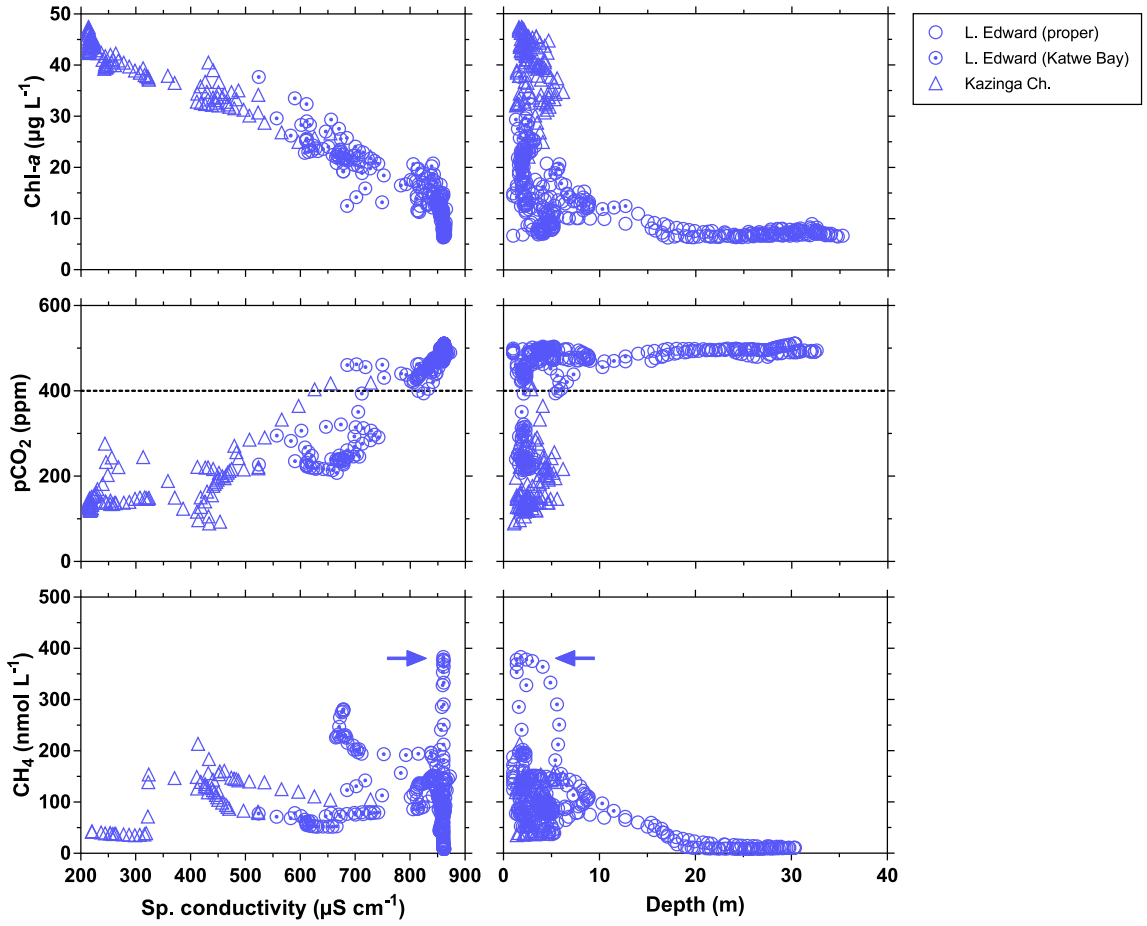

Fig. 6. Variations in surface waters of Lake Edward (proper and Katwe Bay) and lower Kazinga Channel of Chlorophyll-*a*, (Chl-*a* in µg/L), partial pressure of CO_2 (pCO_2, ppm), CH_4 concentration (nmol/L), N_2O saturation level ($\%N_2O$, %) in March 2019. Horizontal dotted line indicates the atmospheric equilibrium value.

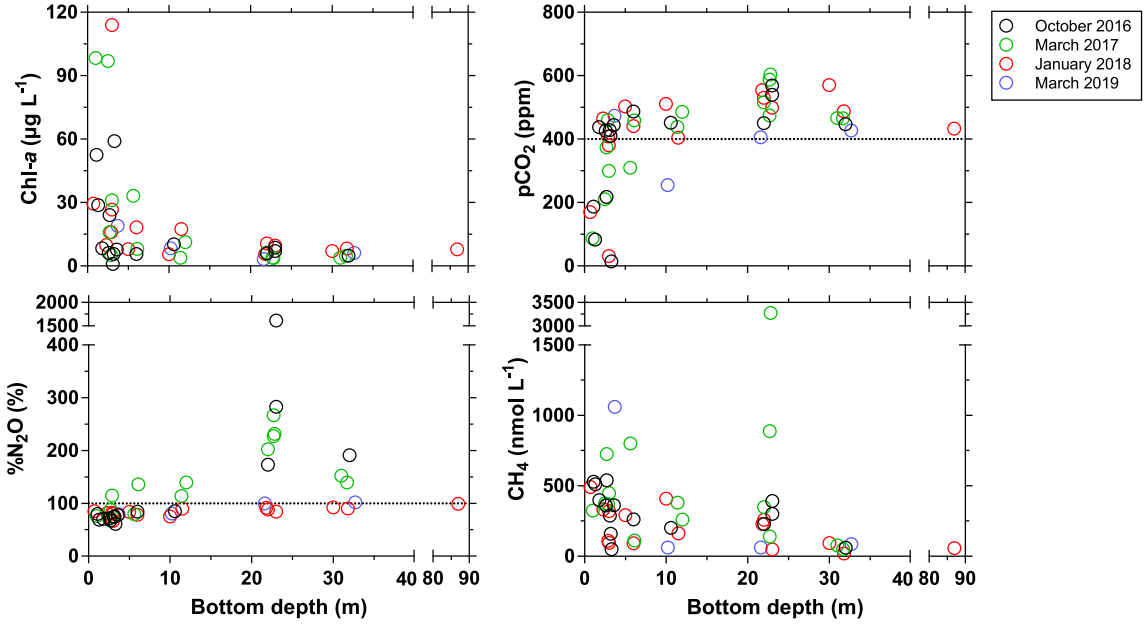

Fig. 7. Variations in surface waters of Lake Edward (for specific conductivity > 800 µS cm^{-1}) of Chlorophyll-*a* (Chl-*a*, µg/L), partial pressure of CO_2 (pCO_2, ppm), N_2O saturation level ($\%N_2O$, %), and CH_4 concentration (nmol/L) as function of bottom depth (m) in October 2016, March 2017, January 2018, March 2019. Horizontal dotted line indicates the atmospheric equilibrium value.

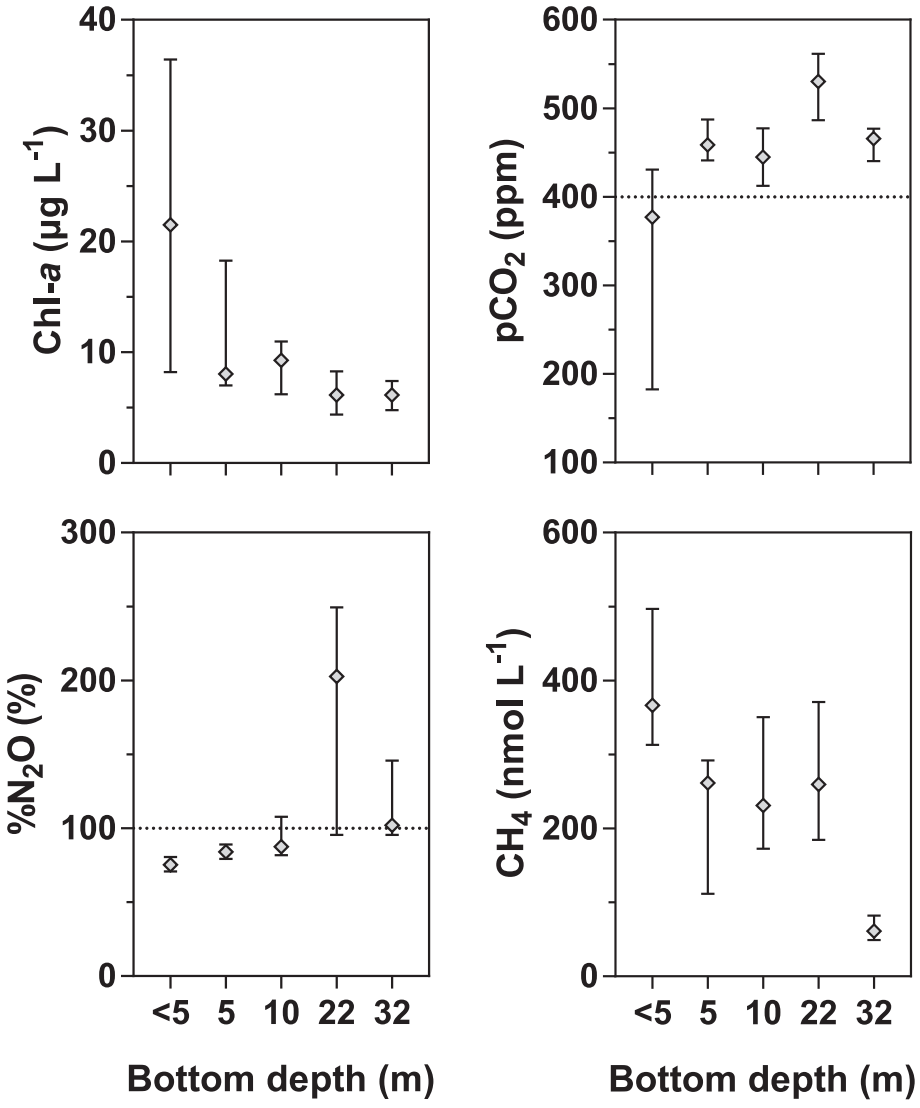

Fig. 8. Variations in surface waters of Lake Edward (for specific conductivity > 800 µS cm^{-1}) of Chlorophyll-*a* (Chl-*a*, µg/L), partial pressure of CO_2 (pCO_2, ppm), N_2O saturation level ($\%N_2O$, %), and CH_4 concentration (nmol/L) as function of bottom depth (m) Horizontal dotted line indicates the atmospheric equilibrium value. Data from October 2016, arch 2017, January 2018, and March 2019 were binned (median) per class of bottom depth. Error bars represent first and third interquartile.

water from layers deeper than 22 m by upward advection, by an upwelling-like process. This is consistent with the fact that wind during the storm was westward (not shown). In addition to inducing vertical mixing, wind should also have entrained surface water from the eastern side of the lake towards the western side.

The CH_4 concentration in surface waters on March 30 (3,277 nmol/L) increased by one order of magnitude compared to March 26 (350 nmol/L). However, one day later (March 31), CH_4 had already dramatically decreased (888 nmol/L) both in surface waters and at 15 m (Fig. 11). The decrease of CH_4 in surface waters between the two samplings on March 30 and 31 corresponds to a removal of 2,520 nmol/L d^{-1} which is very close to the value of methane oxidation measured on March 30, by incubation, of 2,610 nmol/L d^{-1} (data not shown, Borges et al., in unpublished data). The strong increase of $\delta^{13}C$-CH_4 on March 31 (-20.5 ‰) compared to March 30 (-51.3 ‰) was also consistent with a decrease of CH_4 by methane oxidation. The observed $\delta^{13}C$-CH_4 value in surface waters on March 31 (-20.5 ‰) was very close to the value of −20.6 ‰ that can be predicted using a fractionation model based on a Rayleigh equation (Snover and Quay 2000) from CH_4 concentration (20,625 nmol/L) and the $\delta^{13}C$-CH_4 (-56.5 ‰) values at 20 m on March 30 m and a fractionation factor due to methane microbial oxidation of 1.012 empirically derived from incubations in Lake Kivu by Morana et al., (2015).

In October 2017, an extremely high value of $\%N_2O$ (1,616 %) was observed in surface waters of Lake Edward at a station with 22 m bottom depth (Fig. 7). Compared to other samples in surface waters collected during this cruise, the high $\%N_2O$ value was related to lower water temperature and $\%O_2$, and, higher pCO_2, indicating that the high $\%N_2O$ was related to a mixing event (Fig. 12). The sampling was carried on to November 4, two days after a 3-day spell of very windy conditions (maximum 10 min average of 12.5 m s^{-1}), and the day after a severe drop of air temperature (decrease of 4.4 °C of the maximum daily value compared to the day before) (ESM Fig S7). This was confirmed by the comparison of vertical profiles obtained a few days before, on October 23 and 25 (Fig. 13). Both water temperature and specific conductivity profiles indicate mixing conditions on November 4 compared to October 23 and 25. This was consistent with the increase of CH_4, pCO_2, $\%N_2O$ and NO_3^- and the decrease of $\%O_2$ in surface waters on November 4 compared to October 23 and 25. The total vertical mixing of the water mass at 22 m bottom depth would have led to

a final specific conductivity of 854 μS cm^{-1} based on the vertical profile obtained on October 23, which is lower than the actual specific conductivity measured on November 4 of 859 μS cm^{-1}.

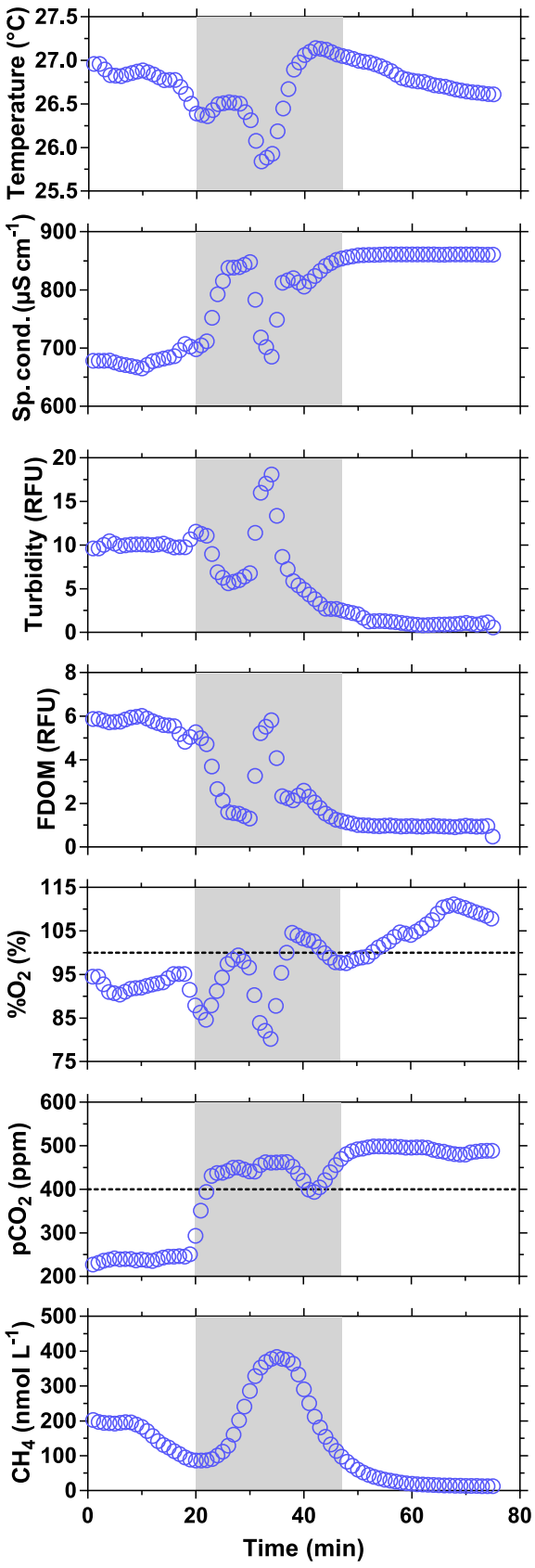

This suggests that in addition to vertical mixing alone, the water mass at 22 m bottom depth on November 4 also resulted in part from the advection of water masses from deeper layers of the lake, as also suggested for the mixing event in March 2017 (see above).

The advection of water masses from deeper layers of the lake is confirmed by the fact that $\%N_2O$ and NO_3^- in surface waters on November 4 were distinctly higher than the water column average at 22 m bottom depth prior to the mixing event on October 23. The increase of $\%N_2O$ observed on November 4 should have then resulted from vertical mixing of water masses, but could have also resulted from nitrification that led to low NH_4^+ in surface waters (Fig. 13). Based on simple two-end mixing model using specific conductivity as a tracer and using as end-members the NH_4^+ at 30 m bottom depth (profile of October 25) and NH_4^+ in surface waters at 22 m bottom depth, a theoretical concentration of NH_4^+ of 4.0 μmol/L should have resulted from mixing. The observed NH_4^+ concentration in surface waters on November 4 was 0.5 μmol/L, the difference resulting most likely from nitrification. The production of N_2O resulting from the oxidation of 3.5 μmol/L of NH_4^+ should have been about 10 nmol/L, using a yield of N_2O production of 0.3 % of oxidized NH_4^+ by nitrification (de Wilde and de Bie, 2000 and references therein). The observed increase of N_2O concentration on November 4 was one order of magnitude higher (around 100 nmol/L). This suggests that the increase of $\%N_2O$ on November 4 mainly resulted from the inputs of N_2O by mixing from bottom waters (rather than nitrification in response to the pulse of NH_4^+ input from mixing). This is consistent with the alignment of N_2O concentrations as a function of conductivity observed on November 4 and the N_2O concentrations in bottom water at the stations at 22 m and 32 m bottom depth (ESM Fig. S8).

The CH_4 concentration in surface water on November 4 was only 392 nmol/L, higher than prior to the mixing event (230 nmol/L on October 23) and could have been potentially higher given that bottom water concentrations ranged between 3,606 nmol/L and 10,514 nmol/L prior to the mixing event (Fig. 13). The sample on November 4 was acquired 2 days after the windy weather (ESM Fig. S7) so that methane oxidation should have already reduced the CH_4 content that would have resulted from mixing, as discussed above for the mixing event in March 2017.

The increase of $\%N_2O$ resulting from the mixing was relatively modest in March 2017 (~30 %) compared to October 2016 (~1,443 %). This can be explained by the very different $\%N_2O$ values in bottom waters at the start and end of rainy season (Fig. 3). In October 2016, the $\%N_2O$ values were extremely high in anoxic waters but very low in March 2017, so that the increase of $\%N_2O$ in March 2017 was mainly related to inputs of water with a high content of N_2O associated to the oxycline, and the resulting increase was mitigated by additional mixing of anoxic waters with a low N_2O content.

During both mixing events (March 2017 and October 2016), pCO_2 levels in surface waters increased by ~90 ppm, which corresponded to a modest increase of ≤ 20 % from the pCO_2 levels prior to the mixing event, compared to CH_4 and $\%N_2O$ that both increased by an order of magnitude in response to the mixing. This is consistent with the fact that at 20 m, the increase of pCO_2 between surface and bottom waters was also modest (~100 ppm) compared to $\%N_2O$ and CH_4 (Figs. 11 and 13).

Fig. 9. Variations in surface waters of Lake Edward of water temperature (temp., °C), specific (Sp.) conductivity (cond., μS cm^{-1}), Turbidity (relative fluorescence units (RFU)), fluorescent dissolved organic matter (FDOM, RFU), O_2 saturation level ($\%O_2$, %), partial pressure of CO_2 (pCO_2, ppm), CH_4 concentration (nmol/L) as a function of time. in March 2019. Horizontal dotted line indicates the atmospheric equilibrium value. Grey area indicates a section of transect presumably influenced by inputs from the Nyamugasani river is indicate in grey (also as triangle in Fig. 4).

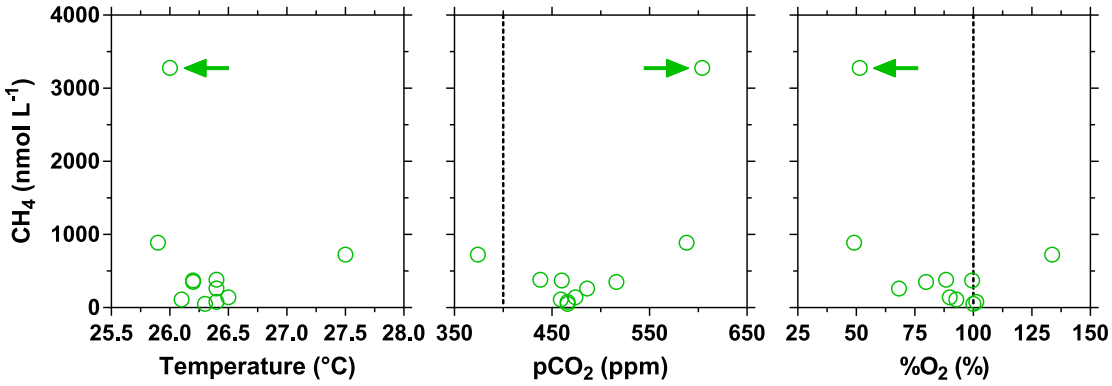

Fig. 10. Variations in surface waters of Lake Edward (for specific conductivity >800 µS cm^{-1}) of CH_4 concentration (nmol/L) as function of water temperature (°C), partial pressure of CO_2 (pCO_2, ppm), O_2 saturation level ($\%O_2$, %) in March 2017. Vertical dotted line indicates the atmospheric equilibrium value. Arrow indicates a particularly elevated CH_4 concentrations measured at a station with a bottom depth of 22 m on March 30.

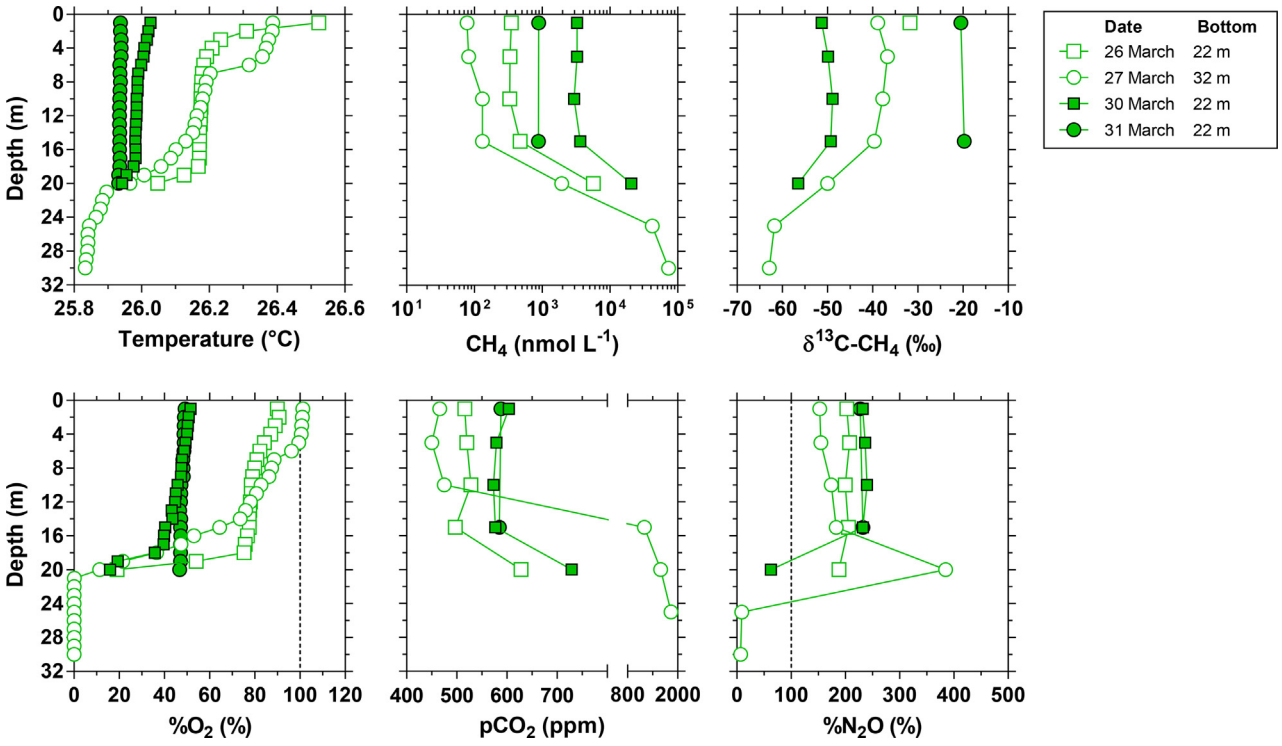

Fig. 11. Vertical profiles of water temperature (°C), CH_4 concentration (nmol/L), carbon stable isotopic composition of CH_4 ($\delta^{13}C$-CH_4, ‰), O_2 saturation level ($\%O_2$, %), partial pressure of CO_2 (pCO_2, ppm), N_2O saturation level ($\%N_2O$, %) in Lake Edward (22 or 32 m bottom depth) on 26/03/2017 (11:00 local time (LT)), 27/03/2017 (09:35 LT), 30/03/2017 (12:55 LT) and 31/03/2017 (14:40 LT). Vertical dotted line indicates the atmospheric equilibrium value.

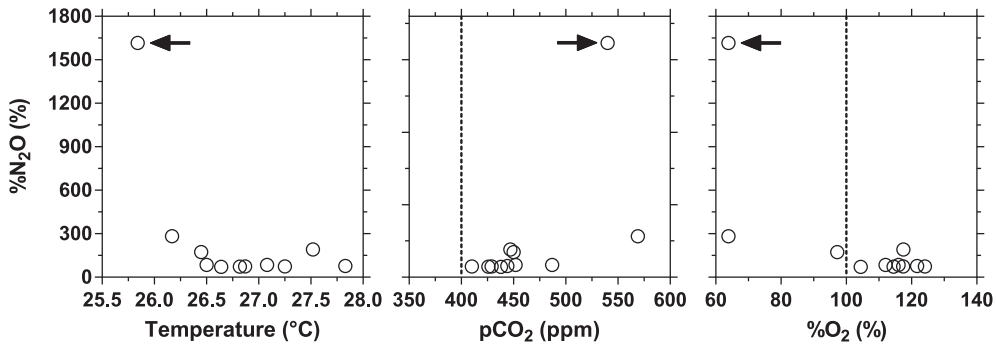

Fig. 12. Variations in surface waters of Lake Edward (for specific conductivity >800 µS cm^{-1}) of N_2O saturation level ($\%N_2O$ in %) as a function of water temperature (°C), partial pressure of CO_2 (pCO_2, ppm), O_2 saturation level ($\%O_2$, %) in October 2016. Vertical dotted line indicates the atmospheric equilibrium value. Arrow indicates a particularly elevated $\%N_2O$ value measured at a station with a bottom depth of 22 m on November 4.

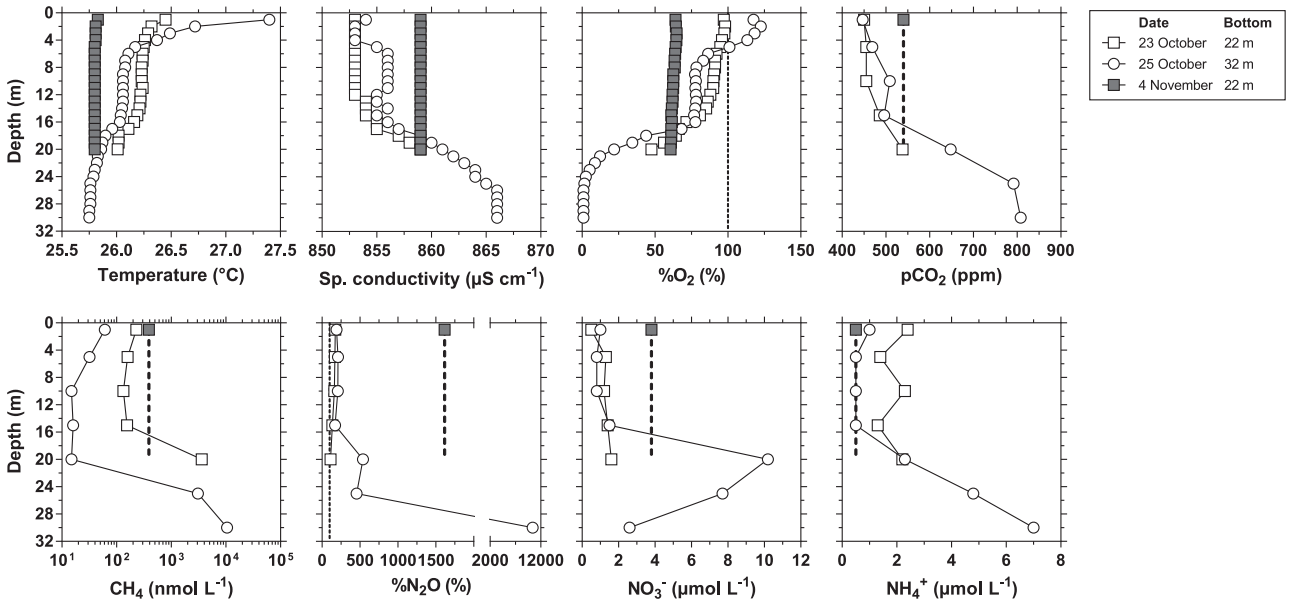

Fig. 13. Vertical profiles of water temperature (°C), specific (Sp.) conductivity (µS cm-1), O_2 saturation level (%O_2, %), partial pressure of CO_2 (pCO_2, ppm), CH_4 concentration (nmol/L), N_2O saturation level (%N_2O, %), NO_3^-, and NH_4^+ concentrations (µmol/L) in Lake Edward (22 or 32 m bottom depth) on 23/10/2016 (10:15 local time (LT)), 25/10/2016 (13:10 LT), and 04/11/2016 (10:15 LT). Fine vertical dotted line indicates the atmospheric equilibrium value, thick vertical dotted line indicates potential values in November 4 assuming a homogeneous vertical profile which was the case for water temperature, Sp. Conductivity and %O_2.

It is notable that these short-term changes of N_2O and CH_4 content in surface waters related to storm-induced mixing were observed on both occasions at stations sampled at 22 m. This corresponds to the depth of the seasonal thermocline (Figs. 2 and 3), meaning that locations shallower than 22 m were mostly permanently vertically mixed, and locations deeper than 22 m probably remained partly stratified and did not fully mix to the bottom after a short-term mixing event during the rainy season. Note that Lewis (1983) suggested that the boundary between continuous and discontinuous mixing was in general at ~20 m depth in lakes with at least 25 km fetch.

Seasonal variations

From January 2017 to December 2019, a shallow station (3 m bottom depth) and a deeper station (22 m bottom depth) were regularly sampled, every 21 d in 2017 and 2018, and every 30 d in 2019. At the deeper station, we observed irregular changes of the potential energy anomaly (PEA) calculated from density gradients according to Simpson (1981) (Fig. 14). This quantity provides a measure of the strength of water column stratification, with a null PEA value indicating fully mixed conditions, and increasing positive values indicating increasing water column stability (e.g., Simpson et al., 2014). The variations of PEA could reflect a combination of changes in thermal stratification at daily scale or at longer time scales (days to weeks). We investigated changes of the thermal vertical gradients at sub-daily scale in Lake Edward at 10 m bottom depth in March 2019 (ESM Fig. S9). During the two days of observations, vertical gradients of temperature up to 1.5 °C occurred in the top 5 m from around 11:00 to dusk, and dissipated during the night, as typically observed in tropical lakes (MacIntyre et al., 2014; Augusto-Silva et al., 2019). The majority of temperature vertical profiles shown in Fig. 14 were carried out during the morning (ESM Table S1). Consequently, changes of PEA mainly reflect variations of stratification at time scales of days to weeks. The variations of PEA indicated an alternation between stratified and mixed conditions but without a clear seasonality (Fig. 14). This was possibly related to the fact that the depth of the seasonal thermocline was located at around 22 m, as mentioned above, so small changes in weather conditions allowed either the establishment or the disintegration of stratification at 22 m bottom depth. Indeed, the boundary between continuous and discontinuous mixing in lakes is in general at ~20 m depth (Lewis, 1983).

Two periods of marked and relatively sustained mixed conditions were observed in January-April 2018 and August-September 2018 (Fig. 14). During these two periods, water temperature, %O_2, CH_4 and %N_2O were relatively homogeneous vertically. During the other sampled periods, moderate to strong vertical gradients were observed in all sampled variables. Maximum bottom water CH_4 values were 14,994 and 23,760 nmol/L in June 2017 and May 2018, respectively, and corresponded to fully anoxic conditions (Fig. 14). The maximum %N_2O values were also observed on these two occasions with a value of 833 % located at the oxycline in June 2017 at 15 m while the anoxic bottom waters were characterized by lower %N_2O (32 %). In May 2018, a value of 1,032 % in %N_2O was observed at 20 m depth in the anoxic layer. This pattern of high/low %N_2O in anoxic waters at the onset/end of a stratified period fits with the %N_2O patterns observed in October 2016 and March 2017 at the station at 32 m bottom depth (Fig. 3).

Fig. 15 shows the variations of pCO_2, CH_4, and %N_2O in surface waters at the shallow and deeper stations (3 and 22 m bottom depth, respectively). Average CH_4 in surface waters was distinctly higher at the shallow station (720 ± 424 nmol/L) than at the deeper station (121 ± 151 nmol/L), while the opposite pattern was observed for %N_2O (90 ± 19 % versus 133 ± 40 %) (Fig. 15). Differences in pCO_2 between the two stations were less marked, yet the average value was lower at the shallower station (466 ± 126 ppm) where values below atmospheric equilibrium were observed on 12 occasions while in the deeper station (540 ± 103 ppm) values below atmospheric equilibrium were only observed on one occasion (Fig. 15). The seasonal variability of pCO_2 was strongly related to phytoplankton biomass, as shown by the negative relationship between pCO_2 and Chl-*a* or POC (Fig. 16), consistent with the uptake of CO_2 by photosynthesis. The average Chl-*a* was distinctly higher at the shallower station (17 ± 8 µg/L)

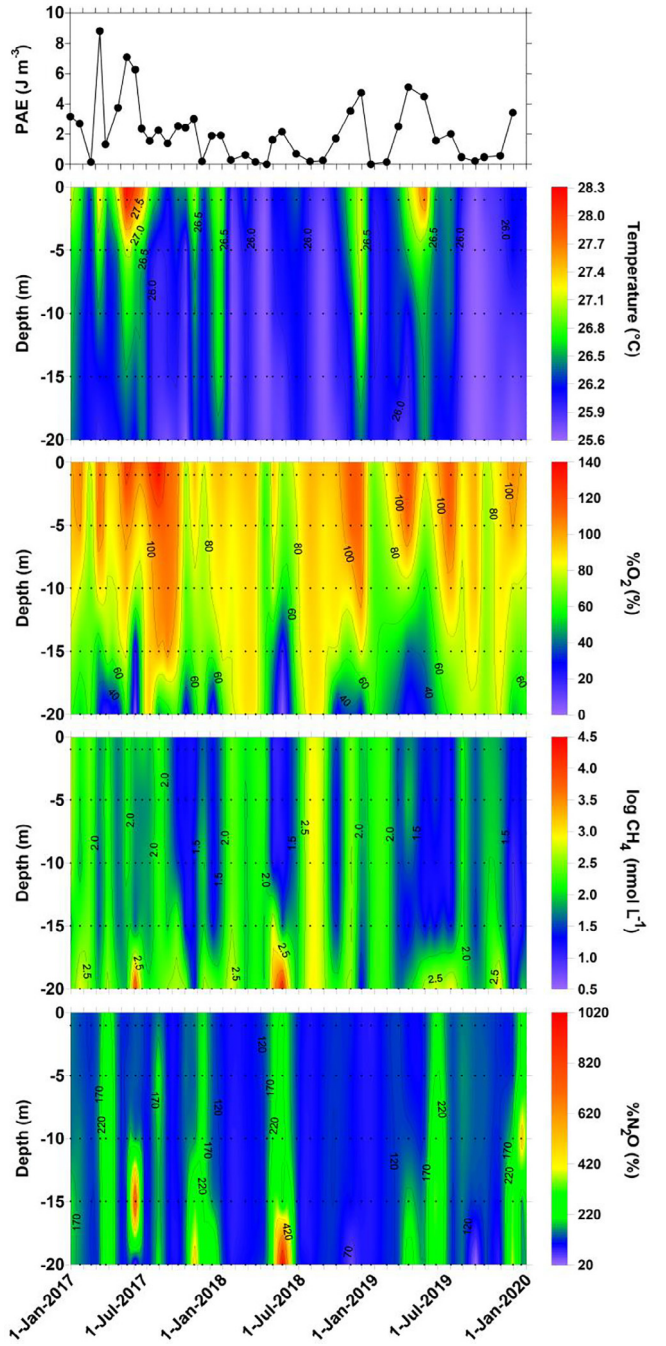

Fig. 14. Potential energy anomaly (PEA, J m^{-3}) computed from density gradients (Simpson, 1981), vertical profiles of water temperature (°C), O_2 saturation level (% O_2, %), log of CH_4 concentration (nmol/L), N_2O saturation level (%N_2O, %) from January 2017 to December 2019 in Lake Edward at a station with bottom depth of 22 m. Dates and time of sampling are given in ESM Table S1.

than at the deeper station (8 ± 3 μg/L). Overall, these differences among the two stations of pCO_2, CH_4 and %N_2O were consistent with the patterns as a function of depth derived from the spatial surveys (Figs. 7 and 8).

The CH_4 concentration at the shallower station did not correlate with Chl-*a* and in fact was negatively correlated to POC (Fig. 16). This could be in part related to the fact that the data points from the most littoral station corresponding to the highest Chl-*a* values might have been influenced by water from the Kazinga Channel, which also had a lower CH_4 content (Fig. 5). Given the strong contribution of the cyanobacteria to total phytoplankton biomass in Lake Edward (Stoyneva-Gaertner et al., 2020) that are producers of CH_4 according to Bižić et al., (2021), the lack of correlation between CH_4 and Chl-*a* indirectly confirms that CH_4 production in aerobic conditions is a marginal flux compared to input fluxes of CH_4 from the sediments (Morana et al., 2020).

The variations among samplings at the deeper station of %N_2O in surface waters and the water column average of %N_2O correlated negatively with %O_2 in the bottom layer (20 m) (Fig. 17). The %O_2 in the bottom layer was in turn correlated to the PEA (ESM Fig. S10). This indicates that the lowering of O_2 content in bottom waters related to stratification promotes the production of N_2O, in particular at the oxycline (Mengis et al., 1997).

Comparison with other lakes

The pCO_2 levels in both Lake George (26 ± 16 ppm) and Edward (404 ± 145 ppm) were lower than values previously attributed in the literature to tropical lakes in general ~1,900 ppm (Marotta et al., 2009; Aufdenkampe et al., 2011; Raymond et al., 2013) and for African lakes specifically, 934 ppm (Raymond et al., 2013) and 2,296 ppm (Cole et al., 1994). This discrepancy most probably results from an over-representation in the literature of studies of South American floodplain lakes and/or of small water bodies, as well as possible methodological over-estimation of pCO_2 values in older studies, computed from pH and TA (Abril et al., 2015). The particularly high pCO_2 average (2,296 ppm) reported by Cole et al., (1994) for African lakes corresponds to 39 lakes located in Cameroon formed in volcanic basins (Kling 1988), some of which are strongly enriched in magmatic and volcanic CO_2 (Kling et al., 1987). The CH_4 levels we report in Lakes George and Edward were within the range previously reported for tropical lakes (Bastviken et al., 2011; Panneer Selvam et al., 2014; Barbosa et al., 2016; Mendoza-Pascual et al., 2021). The N_2O levels were generally low, either slightly below (~80 %) or above saturation (~139 %) in Lakes George and Edward, respectively. This contrasts with previous reports of high N_2O levels in boreal lakes, distinctly above saturation (~270 %; Soued et al., 2015; Kortelainen et al., 2020). This difference of N_2O levels in boreal and tropical lakes might be due to higher levels of denitrification (and removal of N_2O due to complete reduction to N_2) in tropical lakes related to higher temperature (Lewis, 2002). Higher temperature promotes the more frequent occurrence and a longer duration of hypolimnetic anoxia according to Lewis (2002), as well as the metabolic rate of sedimentary denitrification (e.g. Myrstener et al., 2016; Palacin-Lizarbe et al., 2018). Furthermore, high temperatures promote complete denitrification (reduction to N_2 and N_2O removal) while low temperatures promote incomplete denitrification (N_2O accumulation) (Liao et al., 2018).

Conclusions

The content in CO_2, CH_4 and N_2O was different in Lakes George and Edward. The eutrophic Lake George showed lower pCO_2, CH_4 and %N_2O levels (26 ± 16 ppm, 234 ± 208 nmol/L, 80 ± 9 %) than Lake Edward (404 ± 145 ppm, 357 ± 483 nmol/L, 139 ± 222 %). Variations of CO_2, CH_4 and N_2O levels between cruises and between stations were modest. The high cyanobacterial biomass is a permanent feature in Lake George (Ganf and Viner, 1973; Greenwood, 1976) and enables relatively uniform levels in time and space of CO_2, CH_4 and N_2O. The high phytoplankton biomass led to low CO_2 levels, well below atmospheric equilibrium (~390 ppm) due to the uptake by photosynthesis. The strong input of organic matter from phytoplankton detritus to the sediment stimulated denitrification that led to a removal of N_2O from the water column and low %N_2O levels.

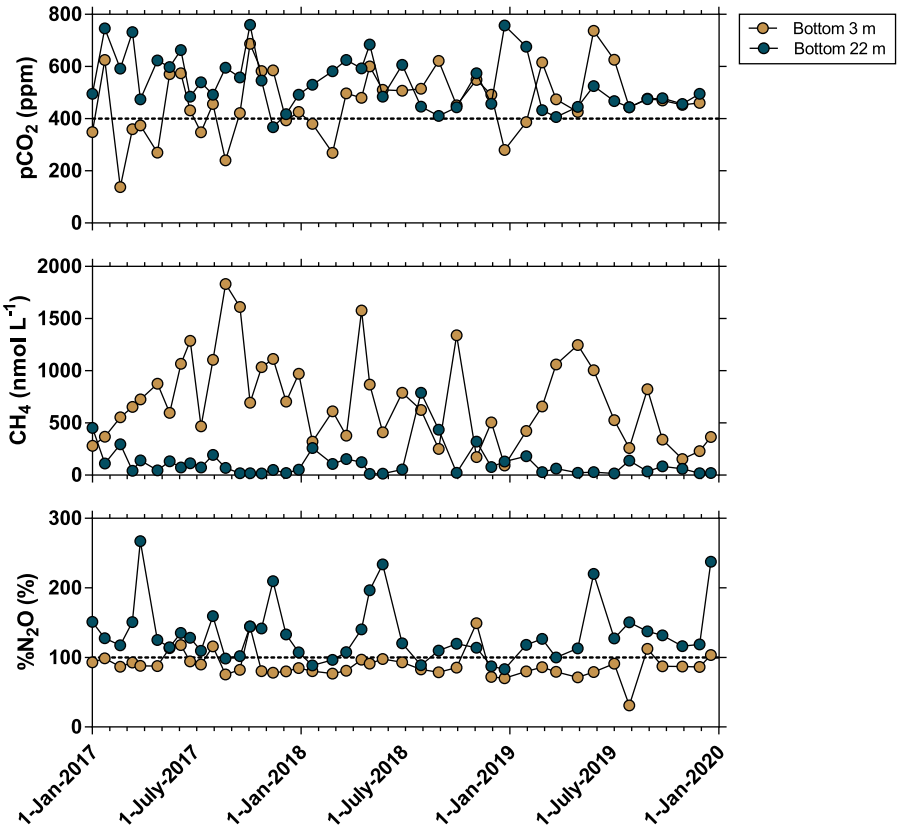

Fig. 15. Variations in surface waters of Lake Edward of the partial pressure of CO_2 (pCO_2, ppm), CH_4 concentration (nmol/L), N_2O saturation level ($\%N_2O$, %) from January 2017 to December 2019. two stations with bottom depth of 3 m and 22 m.

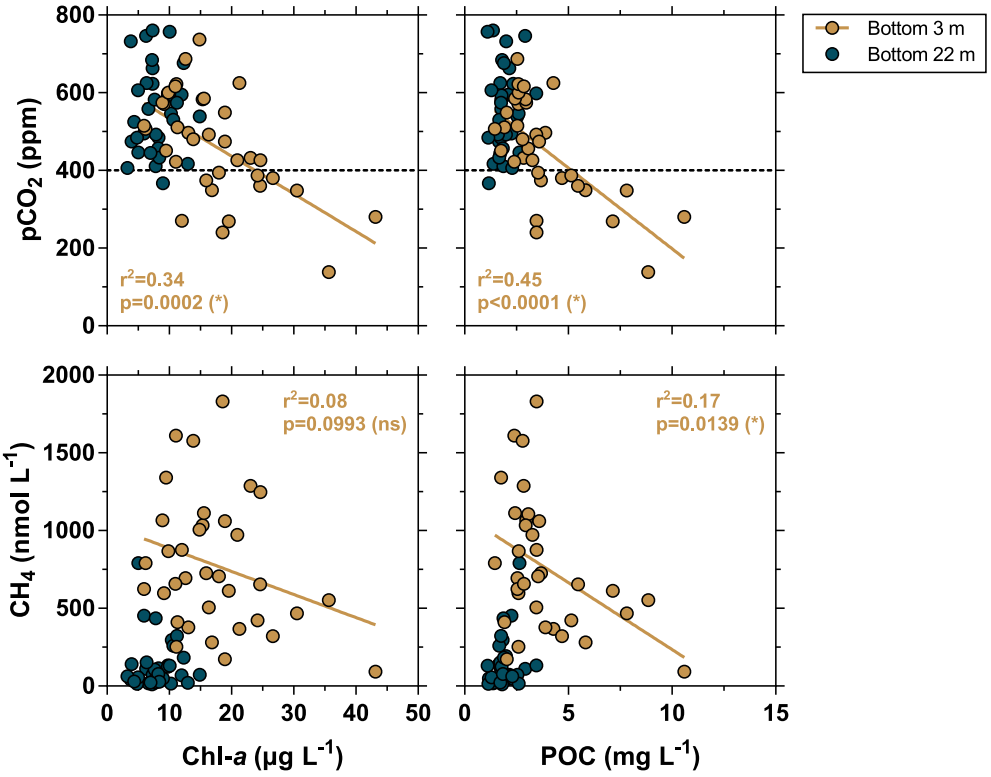

Fig. 16. Partial pressure of CO_2 (pCO_2, ppm) and CH_4 concentration (nmol/L) versus Chlorophyll-a (Chl-*a*, µg/L) and particulate organic carbon (POC, mg L^{-1}), N_2O saturation level ($\%N_2O$, %) in surface waters of Lake Edward, from January 2017 to December 2019, at two stations with bottom depth of 3 m and 22 m.

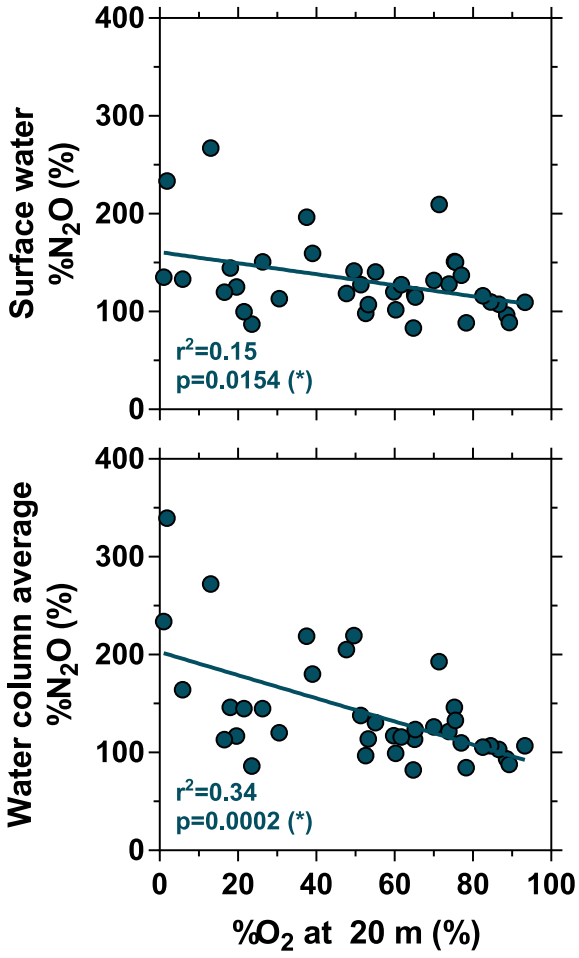

Fig. 17. N_2O saturation level (%N_2O, %) in surface waters and the water column average versus the O_2 saturation level (%O_2, %) in bottom waters (sampled at 20 m depth) in Lake Edward, at a station with bottom depth of 22 m, from January 2017 to December 2019.

In Lake Edward, strong seasonal variations of CO_2, CH_4 and N_2O levels were observed in bottom waters in relation to presence or absence of anoxia that was itself related to occurrence of stratified or mixed conditions. In surface waters, the spatial variations of CO_2, CH_4 and N_2O were mainly related to bottom depth. Shallow waters were characterized by higher phytoplankton biomass, leading to low pCO_2 and %N_2O values (below atmospheric equilibrium) but to high CH_4. Despite the fact that the organic matter content in sediments and sediment–water fluxes of CH_4 were much higher in Lake George than in Lake Edward, the CH_4 concentration in surface waters of Lake George were lower than in Lake Edward at similar depths. This difference could be explained by higher methane oxidation in Lake George compared to Lake Edward. In addition to seasonal variations, short-term extreme mixing events related to storms led to the increase of CO_2, CH_4 and N_2O content in surface waters, that was particularly marked on some occasion for CH_4 and N_2O but more modest for CO_2, as vertical gradients of CH_4 and N_2O (on some occasions) were much more intense than for CO_2. The increase of CH_4 in surface waters was transient, and a tremendous decrease in CH_4 could occur at the scale of one day due to intense methane oxidation. For CH_4, we also observed a localized large increase in near-shore waters of Lake Edward due to flooding of a river in response to storm events. Overall, this indicates that CH_4 and N_2O emissions to the atmosphere from tropical lakes can have 'hot moments' (McClain et al., 2003), as previously reported in boreal lakes but due to different mechanisms (ice thawing). While such hot moments could be seasonal in boreal lakes since ice thawing only occurs once during the year, they could be frequent in tropical lakes, as vertical thermal gradients are often weak, and stratification can frequently be eroded by storm events. Further investigation and quantification of these hot moments will require a mooring-based approach rather than a snap-shot survey approach as used in the present study. Overall, this calls for large scale sampling effort to better characterize CO_2, CH_4 and N_2O across the full range of tropical lakes in terms of climate, watershed characteristics, and morphology (size and depth).

Declaration of Competing Interest

The authors declare that they have no known competing financial interests or personal relationships that could have appeared to influence the work reported in this paper.

Acknowledgments

This work was funded by the Belgian Federal Science Policy Office (contract BR/154/A1/HIPE), with additional financial support for travel grants to AVB, SB, CM, from the Fonds National de la Recherche Scientifique (FNRS), Fonds Wetenschappelijk Onderzoek (FWO), and the Fonds Agathon de Potter. We are grateful to the Katwe marine police, the Uganda Wildlife Authority (UWA) and the Institut Congolais Pour la Conservation de la Nature (ICCN) for help during sampling, to Marc-Vincent Commarieu, Zita Kelemen, and Thomas Bousmanne for analytical support, and comments from one anonymous reviewer. LD, TL, and CM were postdoctoral researchers at the FNRS and AVB is a Research Director at the FNRS.

Appendix A. Supplementary data

Supplementary data to this article can be found online at https://doi.org/10.1016/j.jglr.2022.11.010.

References

Abraham, J., Allen, P.M., Dunbar, J.A., Dworkin, S.I., 1999. Sediment type distribution in reservoirs: sediment source versus morphometry. Env. Geol. 38, 101–110.

Abril, G., Guérin, F., Richard, S., Delmas, R., Galy-Lacaux, C., Gosse, P., Tremblay, A., Varfalvy, L., Aurelio Dos Santos, M., Matvienko, B., 2005. Carbon dioxide and methane emissions and the carbon budget of a 10-year old tropical reservoir (Petit Saut, French Guiana). Global Biogeochem. Cycles 19, GB4007, 10.1029/2005GB002457.

Abril, G., Martinez, J.-M., Artigas, L.F., Moreira-Turcq, P., Benedetti, M.F., Vidal, L., Meziane, T., Kim, J.-H., Bernardes, M.C., Savoye, N., Deborde, J., Albéric, P., Souza, M.F.L., Souza, E.L., Roland, F., 2014. Amazon river carbon dioxide outgassing fueled by wetlands. Nature 505, 395–398.

Abril, G., Bouillon, S., Darchambeau, F., Teodoru, C.R., Marwick, T.R., Tamooh, F., Omengo, F.O., Geeraert, N., Deirmendjian, L., Polsenaere, P., Borges, A.V., 2015. Technical note: Large overestimation of pCO_2 calculated from pH and alkalinity in acidic, organic-rich freshwaters. Biogeosciences 12, 67–78.

Amaral, J.H.F., Borges, A.V., Melack, J.M., Sarmento, H., Barbosa, P.M., Kasper, D., Melo, M.L., de Fex Wolf, D., da Silva, J.S., Forsberg, B.R., 2018. Influence of plankton metabolism and mixing depth on CO2 dynamics in an Amazon floodplain lake. Sci. Total Env. 630, 1381–1393.

Amaral, J.H.F., Melack, J.M., Barbosa, P.M., Borges, A.V., Kasper, D., Cortes, A.C., Zhou, W., MacIntyre, S., Forsberg, B.R., 2022. Inundation, hydrodynamics and vegetation influences carbon dioxide concentrations in Amazon floodplain lakes. Ecosystems 25, 911–930. https://doi.org/10.1007/s10021-021-00692-y.

Apha, 1998. Standard Methods for the Examination of Water and Wastewater. American Public Health Association, Washington DC.

Aufdenkampe, A.K., Mayorga, E., Raymond, P.A., Melack, J.M., Doney, S.C., Alin, S.R., Aalto, R.E., Yoo, K., 2011. Riverine coupling of biogeochemical cycles between land, oceans, and atmosphere. Front. Ecol. Environ. 9, 53–60.

Augusto-Silva, P.B., MacIntyre, S., de Moraes Rudorff, C., Cortés, A., Melack, J.M., 2019. Stratification and mixing in large shallow lakes along the lower Amazon River floodplain. J. Great Lakes Res. 45, 61–72.

Bange, H.W., Sim, C.H., Bastian, D., Kallert, J., Kock, A., Mujahid, A., Müller, M., 2019. Nitrous oxide (N_2O) and methane (CH_4) in rivers and estuaries of northwestern Borneo. Biogeosciences 16, 4321–4335.

Barbosa, P.M., Melack, J.M., Farjalla, V.F., Amaral, J.H.F., Scofield, V., Forsberg, B.R., 2016. Diffusive methane fluxes from Negro, Solimões and Madeira rivers and fringing lakes in the Amazon basin. Limnol. Oceanogr. 61, S221–S237.

Barbosa, P.M., Melack, J.M., Amaral, J.H.F., MacIntyre, S., Kasper, D., Cortés, A., Farjalla, V.F., Forsberg, B.R., 2020. Dissolved CH4 concentrations and fluxes to the atmosphere from a tropical floodplain lake. Biogeochemistry 148, 129–151.

Barros, N., Cole, J.J., Tranvik, L.J., Prairie, Y.T., Bastviken, D., Huszar, V.L.M., del Giorgio, P., Roland, F., 2011. Carbon emission from hydroelectric reservoirs linked to reservoir age and latitude. Nat. Geosci. 4, 593–596.

Bastviken, D., Tranvik, L.J., Downing, J.A., Crill, P.M., Enrich-Prast, A., 2011. Freshwater methane emissions offset the continental carbon sink. Science 331, 50–50.

Beadle, L.C., 1932. Scientific results of the Cambridge Expedition to the East African Lakes 1930–31. 4. The waters of some East African lakes in relation to their fauna and flora. J. Linn. Sot. Zool. 38, 157–211.

Beadle, L.C., 1966. Prolonged stratification and deoxygenation in tropical lakes. I. Crater lake Nkugute, Uganda, compared with Lakes Bunyoni and Edward. Limnol. Oceanogr. 11, 152–163.

Beaulieu, J.J., McManus, M.G., Nietch, C.T., 2016. Estimates of reservoir methane emissions based on a spatially balanced probabilistic-survey. Limnol. Oceanogr. 61, S27–S40.

Begum, M.S., Bogard, M.J., Butman, D.E., Chea, E., Kumar, S., Lu, X., Nayna, O.K., Ran, L., Richey, J.E., Tareq, S.M., Xuan, D.T., Yu, R., Park, J.-H., 2021. Localized pollution impacts on greenhouse gas dynamics in three anthropogenically modified Asian river systems. J. Geophys. Res. Biogeosciences 126. https://doi.org/10.1029/2020JG006124. e2020JG006124.

Beuning, K.R.M., Russell, J.M., 2004. Vegetation and sedimentation in the Lake Edward Basin, Uganda-Congo during the late Pleistocene and early Holocene. J. Paleolimnol. 32, 1–18.

Bižić, M., Klintzsch, T., Ionescu, D., Hindiyeh, M.Y., Günthel, M., Muro-Pastor, A.M., Eckert, W., Urich, T., Keppler, F., Grossart, H.-P., 2021. Aquatic and terrestrial cyanobacteria produce methane. Sci. Adv. 6 (eaax5343), 1–9.

Borges, A.V., Abril, G., Delille, B., Descy, J.-P., Darchambeau, F., 2011. Diffusive methane emissions to the atmosphere from Lake Kivu (Eastern Africa). J. Geophys. Res. 116, G03032. https://doi.org/10.1029/2011JG001673.

Borges, A.V., Morana, C., Bouillon, S., Servais, P., Descy, J.-P., Darchambeau, F., 2014. Carbon cycling of Lake Kivu (East Africa): net autotrophy in the epilimnion and emission of CO_2 to the atmosphere sustained by geogenic inputs. PlosOne 9, e109500.

Borges, A.V., Abril, G., Darchambeau, F., Teodoru, C.R., Deborde, J., Vidal, L.O., Lambert, T., Bouillon, S., 2015a. Divergent biophysical controls of aquatic CO_2 and CH_4 in the World's two largest rivers. Sci. Rep. 5, 15614. https://doi.org/10.1038/srep15614.

Borges, A.V., Darchambeau, F., Teodoru, C.R., Marwick, T.R., Tamooh, F., Geeraert, N., Omengo, F.O., Guérin, F., Lambert, T., Morana, C., Okuku, E., Bouillon, S., 2015b. Globally significant greenhouse gas emissions from African inland waters. Nature Geosci. 8, 637–642.

Borges, A.V., Darchambeau, F., Lambert, T., Morana, C., Allen, G.H., Tambwe, E., Toengaho Sembaito, A., Mambo, T., Nlandu Wabakhangazi, J., Descy, J.-P., Teodoru, C.R., Bouillon, S., 2019. Variations in dissolved greenhouse gases (CO_2, CH_4, N_2O) in the Congo River network overwhelmingly driven by fluvial-wetland connectivity. Biogeosciences 16, 3801–3834.

Borges, A.V., Deirmendjian, L., Bouillon, S., Okello, W., Lambert, T., Roland, F.A.E., Razanamahandry, V.F., Voarintsoa, N.R.G., Darchambeau, F., Kimirei, I.A., Descy, J.-P., Allen, G.H., Morana, C., 2022a. Greenhouse gas emissions from African lakes are no longer a blind spot. Sci. Adv. 8 (eabi8716), 1–17.

Borges, A.V., Morana, C., Okello, W., Bouillon, S., Biogeochemical data from the HIPE project in Lakes Edward and George (East African Rift), Zenodo, version 1, 2022b, 10.5281/zenodo.7263328.

Call, M., Sanders, C.J., Enrich-Prast, A., Sanders, L., Marotta, H., Santos, I.R., Maher, D. T., 2018. Radon-traced pore-water as a potential source of CO_2 and CH_4 to receding black and clear water environments in the Amazon Basin. Limnol. Oceanogr. Lett. 3 (375–383), 2018.

Codispoti, L.A., Christensen, J.P., 1985. Nitirification, denitrification and nitroux oxide cycling in the Eastern tropical South Pacific Ocean. Mar. Chem. 16, 277–300.

Cole, J.J., Caraco, N.F., Kling, G.W., Kratz, T.K., 1994. Carbon dioxide supersaturation in the surface waters of lakes. Science 265, 1568–1570.

Damas, H., 1937. Recherches hydrobiologiques dans les lacs Kivu, Edouard, et Ndalaga. Explor. Part Natl. Albert, Mission H. Damas (1935-36), Fast. I., 128 p. Inst. Parts Natl. Congo Belge.

de Wilde, H.P.J., de Bie, M.J.M., 2000. Nitrous oxide in the Schelde estuary: production by nitrification and emission to the atmosphere. Mar. Chem. 69, 203–216.

del Giorgio, P.A., Peters, R.H., 1994. Patterns in planktonic P: R ratios in lakes: Influence of lake trophy and dissolved organic carbon. Limnol. Oceanogr. 39, 772–787.

DelSontro, T., del Giorgio, P.A., Prairie, Y.T., 2018. No longer a paradox: the interaction between physical transport and biological processes explains the spatial distribution of surface water methane within and across lakes. Ecosystems 21, 1073–1087.

Denfeld, B.A., Wallin, M.B., Sahlée, E., Sobek, S., Kokic, J., Chmiel, H.E., Weyhenmeyer, G.A., 2015. Temporal and spatial carbon dioxide concentration patterns in a small boreal lake in relation to ice-cover dynamics, Boreal Envi. Res. 20, 679–692.

Descy, J.-P., Hardy, M.-A., Sténuite, S., Pirlot, S., Leporcq, B., Kimirei, I., Sekadende, B., Mwaitega, S.R., Sinyenza, D., 2005. Phytoplankton pigments and community composition in Lake Tanganyika. Freshw. Biol. 50, 668–684.

Desrosiers, K., DelSontro, T., del Giorgio, P.A., 2021. Disproportionate contribution of vegetated habitats to the CH_4 and CO_2 budgets of a boreal lake. Ecosystems. https://doi.org/10.1007/s10021-021-00730-9.

Duvert, C., Bossa, M., Tyler, K.J., Wynn, J.G., Munksgaard, N.C., Bird, M.I., Setterfield, S.A., Hutley, L.B., 2019. Groundwater-derived DIC and carbonate buffering enhance fluvial CO2 evasion in two Australian tropical rivers. J. Geophys. Res. 124, 312–327.

Frankignoulle, M., Borges, A., Biondo, R., 2001. A new design of equilibrator to monitor carbon dioxide in highly dynamic and turbid environments. Water Res. 35, 1344–1347.

Ganf, G.G., Viner, A.B., 1973. Ecological stability in a shallow equatorial lake (Lake George, Uganda). Proc. Roy. Soc. B 184, 321–346.

Geeraert, N., Omengo, F.O., Borges, A.V., Govers, G., Bouillon, S., 2017. Shifts in the carbon dynamics in a tropical lowland river system (Tana River, Kenya) during flooded and non-flooded conditions. Biogeochemistry 132, 141–163.

Greenwood, P.H., 1976. Lake George, Uganda. Philos. Trans. R. Soc. London Series B, Biol. Sci. 274, 375–391.

Huttunen, J.T., Alm, J., Liikanen, A., Juutinen, S., Larmola, T., Hammar, T., Silvola, J., Martikainen, P.J., 2003. Fluxes of methane, carbon dioxide and nitrous oxide in boreal lakes and potential anthropogenic effects on the aquatic greenhouse gas emissions. Chemosphere 52, 609–621.

Karlsson, J., Giesler, R., Persson, J., Lundin, E., 2013. High emission of carbon dioxide and methane during ice thaw in high latitude lakes. Geophys. Res. Lett. 40, 1123–1127.

Kling, G.W., 1988. Comparative transparency, depth of mixing, and stability of stratification in lakes of Cameroon, West Africa. Limnol. Oceanogr. 33, 27–40.

Kling, G.W., Clark, M.A., Wagner, G.N., Compton, H.R., Humphrey, A.M., Devine, J.D., Evans, W.C., Lockwood, J.P., Tuttle, M.L., Koenigsberg, E.J., 1987. The 1986 Lake Nyos gas disaster in Cameroon, West Africa. Sience 236, 169–175.

Kortelainen, P., Larmola, T., Rantakari, M., Juutinen, S., Alm, J., Martikainen, P.J., 2020. Lakes as nitrous oxide sources in the boreal landscape. Glob. Change Biol. 26, 1432–1445.

Lauerwald, R., Laruelle, G.G., Hartmann, J., Ciais, P., Regnier, P.A.G., 2015. Spatial patterns in CO_2 evasion from the global river network. Global Biogeochem. Cycles 29, 534–554.

Lewis Jr., W.M., 1983. A revised classification of lakes based on mixing. Can. J. Fish. Aquat. Sci. 40, 1779–1787.

Lewis Jr., W.M., 1987. Tropical limnology. Annu. Rev. Ecol. Systemat. 18, 159–184.

Lewis Jr., W.M., 2002. Causes for the high frequency of nitrogen limitation in tropical lakes. Verh. Internat. Verein. Limnol. 28, 210–213.

Liao, R., Miao, Y., Li, J., Li, Y., Wang, Z., Du, J., Li, Y., Li, A., Shen, H., 2018. Temperature dependence of denitrification microbial communities and functional genes in an expanded granular sludge bed reactor treating nitrate-rich wastewater. RSC Adv. 8, 42087–42094.

Liu, S., Butman, D.E., Raymond, P.A., 2020. Evaluating CO_2 calculation error from organic alkalinity and pH measurement error in low ionic strength freshwaters. Limnol. Oceanogr. Methods 18, 606–622.

Liu, S., Kuhn, C., Amatulli, G., Aho, K., Butman, D.E., Allen, G.H., Ling, P., Pan, M., Yamazaki, D., Brinkerhoff, C., Gleason, C., Xia, X., Raymond, P.A., 2022. The importance of hydrology in routing terrestrial carbon to the atmosphere via global streams and rivers. Proc. Natl. Acad. Sci. USA 119, e2106322119.

MacIntyre, S., 2013. Climatic variability, mixing dynamics, and ecological consequences in the African Great Lakes. In: Goldman, C.R., Kumagai, M., Robarts, R.D. (Eds.), Climatic Change and Global Warming of Inland Waters: Impacts and Mitigation for Ecosystems and Societies. Wiley, pp. 311–336.

MacIntyre, S., Romero, J.R., Silsbe, G.M., Emery, B.M., 2014. Stratification and horizontal exchange in Lake Victoria, East Africa. Limnol. Oceanogr. 59, 1805–1838.

Marotta, H., Duarte, C.M., Sobek, S., Enrich-Prast, A., 2009. Large CO_2 disequilibria in tropical lakes. Global Biogeochem. Cycles 23, GB4022. https://doi.org/10.1029/2008GB003434.

Marra, J., 1997. Analysis of diel variability in chlorophyll fluo-rescence. J. Mar. Res. 55, 767–784.

McClain, M.E., Boyer, E.W., Dent, C.L., Gergel, S.E., Grimm, N.B., Groffman, P.M., Hart, S.C., Harvey, J.W., Johnston, C.A., Mayorga, E., McDowell, W.H., Pinay, G., 2003. Biogeochemical hot spots and hot moments at the interface of terrestrial and aquatic ecosystems. Ecosystems 6, 301–312.

Melack, J.M., Hess, L.L., Gastil, M., Forsberg, B.R., Hamilton, S.K., Lima, I.B.T., Novo, E. M.L.M., 2004. Regionalization of methane emissions in the Amazon Basin with microwave remote sensing. Global Change Biol. 10, 530–544.

Mendonça, R., Müller, R.A., Clow, D., Verpoorter, C., Raymond, P., Tranvik, L.J., Sobek, S., 2017. Organic carbon burial in global lakes and reservoirs. Nat. Commun. 8 (1694), 1–7.

Mendoza-Pascual, M.U., Itoh, M., Aguilar, J.I., Padilla, K.S.A.R., Papa, R.D.S., Okuda, N., 2021. Controlling factors of methane dynamics in tropical lakes of different depths. J. Geophys. Res. Biogeosci. 126. https://doi.org/10.1029/2020JG005828. e2020JG005828.

Mengis, M., Gächter, R., Wehrli, B., 1997. Sources and sinks of nitrous oxide (N_2O) in deep lakes. Biogeochemistry 38, 281–301.

Morana, C., Borges, A.V., Roland, F.A.E., Darchambeau, F., Descy, J.-P., Bouillon, S., 2015. Methanotrophy within the water column of a large meromictic tropical lake (Lake Kivu, East Africa). Biogeosciences 12, 2077–2088.

Morana, C., Bouillon, S., Nolla-Ardèvol, V., Roland, F.A.E., Okello, W., Descy, J.-P., Nankabirwa, A., Nabafu, E., Springael, D., Borges, A.V., 2020. Methane paradox in tropical lakes?. Sedimentary fluxes rather than pelagic production in oxic conditions sustain methanotrophy and emissions to the atmosphere. Biogeosciences 17, 5209–5221.

Morana, C., Borges, A.V., Deirmendjian, L., Okello, W., Sarmento, H., Descy, J.-P., Kimirei, I.A., Bouillon, S., 2022. Prevalence of autotrophy in non-humic African lakes. Ecosystems. https://doi.org/10.1007/s10021-022-00783-4.

Myrstener, M., Jonsson, A., Bergström, A.-K., 2016. The effects of temperature and resource availability on denitrification and relative N_2O production in boreal lake sediments. J. Environ. Sci. 47, 82–90.

Ollivier, Q.R., Maher, D.T., Pitfield, C., Macreadie, P.E., 2022. Net drawdown of greenhouse gases (CO_2, CH_4 and N_2O) by a temperate Australian seagrass meadow. Estuaries Coasts 45, 2026–2039.

Palacin-Lizarbe, C., Camarero, L., Catalan, J., 2018. Denitrification temperature dependence in remote, cold, and N-poor lake sediments. Water Resour. Res. 54, 1161–1173.

Panneer Selvam, B., Natchimuthu, S., Arunachalam, L., Bastviken, D., 2014. Methane and carbon dioxide emissions from inland waters in India - implications for large scale greenhouse gas balances. Glob. Chang. Biol. 20, 3397–3407.

Raymond, P.A., Hartmann, J., Lauerwald, R., Sobek, S., McDonald, C., Hoover, M., Butman, D., Striegl, R., Mayorga, E., Humborg, C., Kortelainen, P., Dürr, H., Meybeck, M., Ciais, P., Guth, P., 2013. Global carbon dioxide emissions from inland waters. Nature 503, 355–359.

Reading, M.J., Maher, D.T., Santos, I.R., Jeffrey, L.C., Cyronak, T.J., McMahon, A., Tait, D.R., 2021. Spatial distribution of CO_2, CH_4, and N_2O in the Great Barrier Reef revealed through high resolution sampling and isotopic analysis. Geophys. Res. Lett. 48, e2021GL092534; 10.1029/2021GL092534.

Richey, J.E., Devol, A.H., Wofy, S.C., Victoria, R., Riberio, M.N.G., 1998. Biogenic gases and the oxidation and reduction of carbon in Amazon River and floodplain waters. Limnol. Oceanogr. 33, 551–561.

Richey, J.E., Melack, J.M., Aufdenkampe, A.K., Ballester, V.M., Hess, L., 2002. Outgassing from Amazonian rivers and wetlands as a large tropical source of atmospheric CO_2. Nature 416, 617–620.

Rosentreter, J.A., Borges, A.V., Deemer, B.R., Holgerson, M.A., Liu, S., Song, C., Melack, J., Raymond, P.A., Duarte, C.M., Allen, G.H., Olefeldt, D., Poulter, B., Battin, T.I., Eyre, B.D., 2021. Half of global methane emissions come from highly variable aquatic ecosystem sources. Nat. Geosci. 14, 225–230.

Russell, J.M., Johnson, T.C., 2006. The water balance and stable isotope hydrology of Lake Edward, Uganda-Congo. J. Great Lakes Res. 32, 77–90.

Sand-Jensen, K., Staehr, P.A., 2007. Scaling of pelagic metabolism to size, trophy and forest cover in small Danish lakes. Ecosystems 10, 127–141.

Santos, I.R., Maher, D.T., Eyre, B.D., 2012. Coupling automated radon and carbon dioxide measurements in coastal waters. Environ. Sci. Technol. 46, 7685–7691.

Schilder, J., Bastviken, D., van Hardenbroek, M., Kankaala, P., Rinta, P., Stotter, T., Heiri, O., 2013. Spatial heterogeneity and lake morphology affect diffusive greenhouse gas emission estimates of lakes. Geophys. Res. Lett. 40, 5752–5756.

Simpson, J.H., 1981. The shelf-sea fronts: Implications of their existence and behaviour. Philos. Trans. R. Soc. Lond. 302, 531–546.

Simpson, J.H., Lucas, N.S., Powell, B., Maberly, S.C., 2014. Dissipation and mixing during the onset of stratification in a temperate lake, Windermere. Limnol. Oceanogr. 60, 29–41.

Sjöberg, Y., Dessirier, B., Ghajarnia, N., Jaramillo, F., Jarsjö, J., Panahi, D.M., Xu, D., Zou, L., Manzoni, S., 2022. Scaling relations reveal global and regional differences in morphometry of reservoirs and natural lakes. Sci. Total Environ. 822, 153510.

Snover, A.K., Quay, P.D., 2000. Hydrogen and carbon kinetic isotope effects during soil uptake of atmospheric methane. Global Biogeochem. Cycles 14, 25–39.

Sobek, S., Tranvik, L.J., Cole, J.J., 2005. Temperature independence of carbon dioxide supersaturation in global lakes. Global Biogeochem. Cycles 19, GB2003, 10.1029/2004GB002264.

Soued, C., del Giorgio, P.A., Maranger, R., 2015. Variability in N_2O fluxes across boreal aquatic networks. Nat. Geosci. 9, 116–120.

Standing committee of Analysts, 1981. Ammonia in waters. Methods for the examination of waters and associated materials.

Stoyneva-Gaertner, M., Morana, C., Borges, A.V., Okello, W., Bouillon, S., Deirmendjian, L., Lambert, T., Roland, F., Nankabirwa, A., Nabafu, E., Darchambeau, F., Descy, J.-P., 2020. Diversity and ecology of phytoplankton in Lake Edward (East Africa): present status and long-term changes. J. Great Lakes Res. 46, 741–751.

Tait, D.R., Maher, D.T., Wong, W.W., Santos, I.R., Sadat-Noori, M., Holloway, C., Cook, P.L.M., 2017. Greenhouse gas dynamics in a salt-wedge estuary revealed by high resolution cavity ring-down spectroscopy observations. Environ. Sci. Technol. 51, 13771–13778.

Teodoru, C.R., Nyoni, F.C., Borges, A.V., Darachambeau, F., Nyambe, I., Bouillon, S., 2015. Spatial variability and temporal dynamics of greenhouse gas (CO_2, CH_4, N_2O) concentrations and fluxes along the Zambezi River mainstem and major tributaries. Biogeosciences 12, 2431–2453.

Verbeke, J., 1957. Recherches écologiques sur la faune des grands lacs de l'est du Congo belge. Bulletin de l'Institut royal des Sciences naturelles de Belgique: Résultats scientifiques de l'exploration hydrobiologique (1952-1954) des lacs Kivu, Edouard et Albert.

Viner, A.B., Smith, I.R., 1973. Geographical, historical and physical aspects of Lake George. Proc. Roy. Soc. B 184, 235–270.

Webb, J.R., Maher, D.T., Santos, I.R., 2016. Automated, in situ measurements of dissolved CO_2, CH_4, and $\delta^{13}C$ values using cavity enhanced laser absorption spectrometry: Comparing response times of air-water equilibrators. Limnol. Oceanogr.: Methods 14, 323-337.

Weiss, R.F., 1981. Determinations of carbon dioxide and methane by dual catalyst flame ionization chromatography and nitrous oxide by electron capture chromatography. J. Chromatogr. Sci. 19, 611–616.

Weiss, R.F., Price, B.A., 1980. Nitrous oxide solubility in water and seawater. Mar. Chem. 8, 347–359.

Wells, N.S., Chen, J.-J., Maher, D.T., Huang, P., Erler, D.V., Hipsey, M., Eyre, B.D., 2020. Changing sediment and surface water processes increase CH4 emissions from human-impacted estuaries. Geochim. Cosmochim. Acta 280, 130–147.

Wit, F., Müller, D., Baum, A., Warneke, T., Pranowo, W.S., Müller, M., 2015. The impact of disturbed peatlands on river outgassing in Southeast Asia. Nat. Commun. 6, 1–9.